LANGMUIR

pubs.acs.org/Langmuir Article

# Aqueous Lyotropic Mesophase Behavior of Gemini Dicarboxylate Surfactants Swollen with *n*-Decane

Carlos M. Baez-Cotto, Grayson L. Jackson, and Mahesh K. Mahanthappa*

Cite This: *Langmuir* 2020, 36, 2307−2321 Read Online

ACCESS | Metrics & More | Article Recommendations | Supporting Information

**ABSTRACT:** We report detailed small-angle X-ray scattering (SAXS) studies of the impact of variable *n*-decane loadings on the lyotropic liquid crystalline (LLC) phase behaviors of homologous bis(tetramethylammonium) gemini didecanoate surfactants **TMA-7*x***, which derive from dimerizing decanoic acid through its $\alpha$-carbon with hydrocarbyl linkers $-(CH_2)_x-$ where $x$ = 3, 4, 5, and 6. **TMA-7*x*** amphiphiles with $x$ = 3 or 5 exhibit a strong propensity to form normal double gyroid (G) LLC network mesophases over wide surfactant hydration ranges, as compared to homologues with $x$ = 4 or 6. On swelling aqueous **TMA-7*x*** LLC mesophases with up to 35 wt % *n*-decane, we demonstrate that odd-carbon linked surfactants ($x$ = 3 or 5) form G and normal double diamond (D) phases over wide water concentration windows with $T$ = 22−100 °C. Complementary studies of decane-swollen **TMA-7*x*** ($x$ = 4 or 6) aqueous LLCs instead demonstrate significantly diminished network phase stability, in favor of hexagonally-packed cylinder phases and a zoo of complex quasispherical micelle packings, which include micellar C14 and C15 Laves phases ($P6_3/mmc$ and $Fd3(-)m$ symmetries, respectively) and high-symmetry hexagonally close packed (HCP) and body-centered cubic (BCC) arrangements. These rich phase behaviors are rationalized in terms of linker length parity-dependent surfactant conformations and the delicate free energy balance that guides the packing of these geometrically anisotropic amphiphiles by minimizing unfavorable water-hydrophobic contacts, maximizing ionic surfactant-headgroup counterion solvation with minimal local variations, and maximizing electrostatic cohesion within these supramolecular assemblies.

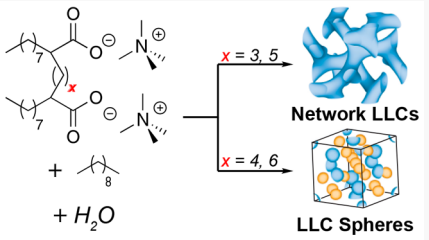




## INTRODUCTION

Small-molecule amphiphiles solvated with small amounts of water self-assemble into ordered one-, two-, and three-dimensional supramolecular assemblies known as lyotropic liquid crystals (LLCs), which comprise spatially periodic aqueous and hydrophobic nanodomains that exhibit long-range translational mesoscopic order.[1−5] The water concentration-dependent LLC morphologies arise from a subtle balance of electrostatic and van der Waals (noncovalent) interactions that direct the constituent amphiphiles into specific interfacial packings, which give rise to unusual bulk physical properties.[6] Judicious manipulation of amphiphile architecture and assembly conditions (i.e., temperature, pressure, *etc.*) leads to mesophases that include ordered 3D packings of discontinuous micelles (I), 2D hexagonally-packed cylinders (H), and 1D lamellar phases ($L_\alpha$).[2,7] These phases are classified as normal (Type I) phases if the aqueous domains curve toward the hydrocarbon domains, while inverse (Type II) LLCs exhibit concave water domains. The formation of LLC mesophases is of fundamental interest and of use in numerous current and prospective applications. Due to their characteristic nanoperiodic hydrophilic and hydrophobic domains, LLCs maybe used as nanoporous polymer membranes,[8−11] structure-directing agents for mesoporous inorganic materials,[12−15] platforms for protein crystallization,[1,16−18] and drug delivery vehicles.[19−21] In some of these applications, the ideal LLC mesophase morphology is a 3D network (N) phase LLC that exhibits percolating and interpenetrating aqueous and hydrophobic domains. Three commonly observed N phases are double gyroid (G), double diamond (D), and primitive (P) morphologies that are built from either 3-, 4-, or 6-fold connectors.[2,22−25] Access to aqueous N phase LLCs derived from single-tail ionic amphiphiles is typically quite limited, thus curtailing the reach of these materials in certain applications. This limitation stems from the inability of such amphiphiles to form negative Gaussian curvature interfacial packings, which require costly variations in headgroup hydration and/or lipid tail packing density.[2] One means of enhancing the stabilities of these N phase aqueous LLCs is to add either hydrophilic or hydrophobic additives in order to relieve the packing frustration associated with such structures.[26−37] Thus, various efforts have sought to identify additives that foster N phase formation and to elucidate their molecular structure/self-assembly relationships.

Extensive work has examined how hydrophobic additives affect the self-assembly of inverse (Type II) N phase LLCs, as a simple means of tuning the structures and stabilities of these

Received: November 4, 2019
Revised: February 10, 2020
Published: February 26, 2020





https://dx.doi.org/10.1021/acs.langmuir.9b03408
*Langmuir* 2020, 36, 2307−2321

potentially useful nanoperiodic structures. Among lipidic LLCs, Type II bicontinuous $G_{II}$ and $D_{II}$ phases have attracted widespread attention as biosensors,[38,39] membrane protein crystallization platforms,[17,18,40−42] and therapeutic delivery vehicles.[43,44] However, their applications scope is sometimes limited by the narrow aqueous pore sizes (e.g., 3−5 nm) that arise from their small unit cell dimensions, with some notable exceptions.[45−47] Although the ability of amphiphiles to stabilize nonlamellar morphologies is poorly rationalized in terms of "critical packing parameter" models,[6,48] assembly of these cubic phases that exhibit negative Gaussian (saddle) curvature is better described as stemming from two competing free-energy terms: (1) the energy associated with interfacial bending and (2) the stretching energy of the surfactant tails.[23,49] This conceptual framework suggests that insertion of hydrophobic additives may serve to reduce the hydrophobic surfactant tail packing frustration to promote greater N phase stability. This notion is confirmed by data compiled in an exhaustive review by Drummond and co-workers[26] that describes the Type II LLC phase behavior of bicontinuous phases bearing different additives, which enhance their stabilities and result in their expanded pore sizes.

In Type I LLCs, however, the effect of hydrophobic additives on $N_I$ phase stabilities and their consequent properties are poorly understood. In the absence of any additives, the interfacial packings adopted by amphiphiles in $N_I$ LLCs are best described as delicately balancing nearly constant surfactant headgroup hydration throughout the assembly, while minimizing variations in hydrophobic tail stretching. Due to the significant deviations from constant mean curvature required for $N_I$ phase formation, the temperature and amphiphile concentration phase windows over which single-tail amphiphile/water mixtures satisfy these packing constraints are quite small, thus limiting access to them. Thus, one might logically seek out additives that stabilize these structures over wider phase windows, by analogy to the aforementioned case of Type II assemblies. In contrast to Type II LLCs, Type I LLCs exhibit a continuous water matrix with convex hydrophobic interfaces. Thus, the impact of additives on the formation of negative Gaussian curvature interfaces with positive mean curvature required for $N_I$ phase self-assembly will be different.

Gemini ("twin head and twin tail") surfactants have recently emerged as new amphiphile architectures that stabilize $N_I$ phases. Work by the groups of Gin[8,9,50−52] and Zana[53] demonstrated that the quaternary phosphonium and quaternary ammonium gemini amphiphiles self-assemble into aqueous LLC $G_I$ phases over phase windows that are ∼10 wt % wide, which are thermally stable between 22−100 °C. These findings were ascribed to the anisotropic nature of the hydrated gemini amphiphiles, which cannot be simply described as axially-symmetric cone structures that pack to fill space. Subsequent work by Mahanthappa and co-workers established that gemini dialkanoate amphiphiles exhibit rich phase behaviors, including their robust ability to self-assemble into lyotropic $G_I$ phases over phase windows as wide as 45 wt % at 22 °C.[54,55] This phase behavior sensitively depends on the length of the surfactant linker, with a pronounced odd/even effect.[55] These findings starkly contrast the phase behaviors of the single-tail alkyl carboxylate surfactants, in which the $N_I$ phase windows are narrow and accessible only at elevated temperatures. Furthermore, gemini dicarboxylates uniquely self-assemble into new $N_I$ phases, such as a tetracontinuous network phase with 3D-hexagonal symmetry ($H_I^{193}$).[56]

The impacts of hydrophobic additives on the phase behaviors of gemini surfactant LLCs, with specific attention to $N_I$ phase stabilization over large phase windows, are poorly investigated. Kunieda and co-workers studied the role of hydrophobic additives in Type I aqueous LLCs of single-tail and gemini alkylamide-based dicarboxylate surfactants, in which two single-tail amphiphiles were linked by an aliphatic $-(CH_2)_2-$ linker.[57] In contrast to the aforementioned gemini dicarboxylates, they surprisingly observed that the binary aqueous LLC $L_\alpha$, $N_I$, and $H_I$ phase window widths were not apparently impacted by the surfactant architecture. The addition of the hydrophobic *n*-dodecane and *m*-xylene typically drove a narrowing of the $H_I$ window and the appearance of a wide region of discontinuous micellar assemblies ($I_I$) for both single-tail and gemini surfactants. The specific $N_I$ and $I_I$ phases formed were not identified, as their analysis relied exclusively on polarized light microscopy (PLM) and low-resolution small-angle X-ray scattering (SAXS). More recently, Jennings et al. demonstrated that gemini dicarboxylate surfactants with hydrocarbyl $-(CH_2)_3-$ linkers and tetramethylammonium charge-compensating counterions exhibit aqueous LLC $G_I$ phase windows that are ∼40 wt % wide.[58] They also demonstrated that these LLC $G_I$ phases could be swelled with the hydrophobic, cross-linkable monomer 1,6-hexanediol dimethacrylate (HDDMA) without diminishing the $N_I$ phase window width. Using high-resolution SAXS, they observed formation of a pure $G_I$ phase as well as two-phase coexistence of $G_I$ and previously unknown normal $D_I$ phases. They further achieved templated cross-linking polymerizations of the diacrylate monomer within the $G_I$ nanostructure to access nanoporous, hydrophobic polymer networks with useful mechanical properties and porosities. The stark differences in these experimental reports on the impact of oil addition on gemini dicarboxylate surfactant LLCs remain poorly understood.

Motivated by these experiments, we report studies of the binary and ternary LLC phase behaviors of tetramethylammonium alkyl carboxylate gemini surfactants, as a function of surfactant linker length in the presence of the hydrophobic additive *n*-decane. We demonstrate that LLCs derived from gemini surfactants with $-(CH_2)_3-$ and $-(CH_2)_5-$ odd-carbon linkers may be swollen with relatively large amounts of *n*-decane (up to 35 wt % overall) to yield pure $G_I$ and pure normal $D_I$ morphologies. Upon swelling LLCs having $-(CH_2)_4-$ or $-(CH_2)_6-$ even-carbon linkers with *n*-decane, a variety of low-symmetry spherical micelle packings emerge. These results are rationalized in terms of surfactant molecular conformations, the extent of counterion-headgroup association, and their resulting supramolecular packings.

## EXPERIMENTAL SECTION

**Materials.** All materials and reagent grade solvents were purchased from Sigma-Aldrich Chemical Co. (Milwaukee, WI, USA) and used as received unless otherwise noted. 1,3-Dibromopropane, 1,4-dibromobutane, 1,5-dibromopentane, and 1,6-dibromohexane were distilled from $CaH_2$ and stored under $N_2$(g), in addition to being shielded from light when possible to minimize photolytic decomposition. Hexamethylphosphoramide (HMPA) was distilled from $CaH_2$ and stored under nitrogen. Anhydrous and anaerobic tetrahydrofuran (THF) was obtained by degassing analytical grade solvent by high purity nitrogen sparging for 30 min, followed by repeated cycling through an activated alumina column for ≥12 h in a Vacuum


https://dx.doi.org/10.1021/acs.langmuir.9b03408
Langmuir 2020, 36, 2307−2321

Atmospheres solvent purification system (Hawthorne, CA). Prior to use, *n*-butyllithium was titrated against a THF solution of diphenylacetic acid. Using a standardized 1.000 N HCl(aq) solution, the concentration of a commercially available tetramethylammonium hydroxide (TMAOH) was determined to be 1.007 M.

**Molecular Characterization.** $^{1}$H and $^{13}$C nuclear magnetic resonance (NMR) spectra of surfactant samples dissolved in $CD_3OD$ were acquired at 23 °C using a Bruker Avance 400 spectrometer. Carbon, hydrogen, and nitrogen combustion analyses were performed by Atlantic Microlab, Inc. (Norcross, GA, USA).

**Gemini Diacid Synthesis.** Gemini diacids derived from *n*-decanoic acid were synthesized by previously reported procedures in yields ranging from 43 to 69%.[54,55]

**Representative Synthesis of Bis(tetramethylammonium) Gemini Surfactants.** In a flask equipped with a stir bar, tetramethylammonium hydroxide (1.007 M, 2 equiv) was added to a suspension of the gemini diacid (1 equiv) in ethanol with an overall reactant concentration ∼0.1−0.2 M.[54,58] The mixture was stirred at 22 °C until it became homogeneous and clear, and then stirring was continued for an additional 2 h. All volatiles were removed under vacuum. The resulting products were azeotropically freeze-dried three times by suspending the solids in $C_6H_6$, freezing the solvent/solid suspension in liquid nitrogen, and removing the $C_6H_6$(s) by sublimation under reduced pressure to furnish the desired material in quantitative yield. Surfactants are identified by the naming convention **TMA-7*x***, where TMA refers to the tetramethylammonium counterion, the number 7 refers to the number of methylene units in the surfactant tail, and *x* is the number of methylene units in the linker (i.e., $-(CH_2)_x-$).

**Tetramethylammonium Heneicosane-9,13-dicarboxylate (TMA-73).** $^{1}$H NMR (400.18 MHz, $CD_3OD$, 24 °C): $\delta$ (ppm) 3.22 (N−*CH*$_3$, s, 24H), 2.20−2.15 (*CH*−COO$^-$, *m*, 2H), 1.60−1.51 (CH−*CH*$_2$, m 4H), 1.42−1.30 (*CH*$_2$, m, 30H), 0.93−0.89 (CH$_2$−*CH*$_3$, t, 6H). $^{13}$C NMR (100.62 MHz, $CD_3OD$, 24 °C): $\delta$ (ppm) 183.8 (C=O), 54.54−54.46 (N(CH$_3$)$_4$), 49.48 (CH), 33.80 (CH$_2$), 33.32 (CH$_2$), 31.70 (CH$_2$), 29.74 (CH$_2$), 29.41 (CH$_2$), 29.10 (CH$_2$), 27.84 (CH$_2$), 26.23 (CH$_2$), 22.35 (CH$_2$), 13.07 (CH$_3$). Batch 1: Anal. Calcd for $C_{31}H_{66}N_2O_4\cdot 1.44\ H_2O$: C, 66.87 H, 12.47; N, 5.03. Found: C, 66.80; H, 12.67; N, 4.97. Batch 2: Anal. Calcd for $C_{31}H_{66}N_2O_4\cdot 2.23\ H_2O$: C, 65.20 H, 12.44; N, 4.92. Found: C, 65.20; H, 12.33; N, 4.92.

**Tetramethylammonium Docosane-9,14-dicarboxylate (TMA-74).** $^{1}$H NMR (400.18 MHz, $CD_3OD$, 24 °C): $\delta$ (ppm) 3.22 (N−*CH*$_3$, s, 24H), 2.18−2.13 (*CH*−COO$^-$, *m*, 2H), 1.59−1.52 (CH−*CH*$_2$, m 4H), 1.35−1.30 (*CH*$_2$, m, 32H), 0.93−0.89 (CH$_2$−*CH*$_3$, t, 6H). $^{13}$C NMR (100.62 MHz, $CD_3OD$, 24 °C): $\delta$ (ppm) 183.85 (C = O), 54.53−54.45 (N(CH$_3$)$_4$), 49.57 (CH), 33.52 (CH$_2$), 32.35 (CH$_2$), 31.69 (CH$_2$), 29.70 (CH$_2$), 29.40 (CH$_2$), 29.09 (CH$_2$), 27.82 (CH$_2$), 26.47 (CH$_2$), 22.34 (CH$_2$), 13.06 (CH$_3$). Batch 1: Anal. Calcd $C_{32}H_{68}N_2O_4\cdot 1.67\ H_2O$: C, 66.85; H, 12.51; N, 4.87. Found: C, 66.94; H, 12.62; N, 4.82. Batch 2: Anal. Calcd $C_{32}H_{68}N_2O_4\cdot 2.00\ H_2O$: C, 66.16; H, 12.49; N, 4.82. Found: C, 66.16; H, 12.32; N, 4.84.

**Tetramethylammonium Tricosane-9,15-dicarboxylate (TMA-75).** $^{1}$H NMR (400.18 MHz, $CD_3OD$, 24 °C): $\delta$ (ppm) 3.22 (N−*CH*$_3$, s, 24H), 2.18−2.14 (*CH*−COO$^-$, *m*, 2H), 1.58−1.51 (CH−*CH*$_2$, m 4H), 1.38−1.30 (*CH*$_2$, m, 34H), 0.93−0.89 (CH$_2$−*CH*$_3$, t, 6H). $^{13}$C NMR (100.62 MHz, $CD_3OD$, 24 °C): $\delta$ (ppm) 183.85 (C=O), 54.54−54.45 (N(CH$_3$)$_4$), 49.54 (CH), 33.56 (CH$_2$), 33.43 (CH$_2$), 31.70 (CH$_2$), 29.71 (CH$_2$), 29.40 (CH$_2$), 29.09 (CH$_2$), 27.84 (CH$_2$), 26.49 (CH$_2$), 22.35 (CH$_2$), 13.08 (CH$_3$). Batch 1: Anal. Calcd for $C_{33}H_{70}N_2O_4\cdot 0.93\ H_2O$: C, 68.85; H, 12.58; N, 4.87. Found: C, 68.81; H, 12.68; N, 4.95. Batch 2: Anal. Calcd for $C_{33}H_{70}N_2O_4\cdot 2.08\ H_2O$: C, 66.46; H, 12.53; N, 4.70. Found: C, 66.46; H, 12.73; N, 4.83.

**Tetramethylammonium Tetracosane-9,16-dicarboxylate (TMA-76).** $^{1}$H NMR (400.18 MHz, $CD_3OD$, 24 °C): $\delta$ (ppm) 3.22 (N−*CH*$_3$, s, 24H), 2.18−2.14 (*CH*−COO$^-$, *m*, 2H), 1.56−1.52 (CH−*CH*$_2$, m 4H), 1.38−1.30 (*CH*$_2$, m, 36H), 0.93−0.89 (CH$_2$−*CH*$_3$, t, 6H). $^{13}$C NMR (100.62 MHz, $CD_3OD$, 24 °C): $\delta$ (ppm) 183.87 (C=O), 54.53−54.44 (N(CH$_3$)$_4$), 49.49 (CH), 33.51 (CH$_2$), 33.41 (CH$_2$), 31.69 (CH$_2$), 29.69 (CH$_2$), 29.39 (CH$_2$), 29.09 (CH$_2$), 27.97 (CH$_2$), 27.82 (CH$_2$), 22.35 (CH$_2$), 13.07 (CH$_3$). Batch 1 Anal. Calcd for $C_{34}H_{72}N_2O_4\cdot 1.11\ H_2O$: C, 68.87; H, 12.62; N, 4.72. Found: C, 68.90; H, 12.88; N, 4.68. Batch 2 Anal. Calcd for $C_{34}H_{72}N_2O_4\cdot 1.75\ H_2O$: C, 67.55; H, 12.59; N, 4.63. Found: C, 67.53; H, 12.84; N, 4.67.

**Preparation of Aqueous Lyotropic Liquid Crystalline (LLC) Samples.** Massed amounts of solid **TMA-7*x*** and *n*-decane (10 or 40 wt % relative to surfactant) were combined in 4 mL vials and mixed by high-speed centrifugation (4950*g*) for 10 min at 25 °C, followed by hand-mixing with a spatula. After repeating this process two more times with the oil/surfactant mixture, ultrapure water (Type I, >18 MΩ·cm) was massed into the mixture using a micropipette. Mixing of this three-component mixture was effected by three additional cycles of centrifugation and hand-mixing to yield optically clear, gel-like solids. To ensure complete and reproducible oil uptake by these mixtures, LLC samples were annealed for 30 min at 50 °C in a thermostated heating block. Finally, samples were allowed to rest at 22 °C for a minimum of 24 h prior to X-ray analyses to relax any residual stresses in the materials and to allow phase nucleation and growth. Samples not in active use were stored in tightly capped vials.

**Small-Angle X-ray Scattering (SAXS).** A beam energy of either 14.0 or 13.3 keV ($\lambda$ = 0.8856 or 0.9322 Å, respectively) and sample-to-detector distance of 2.027 m were used at the Advanced Photon Source (Argonne National Laboratory, Argonne, IL) Sector 12-ID-B synchrotron beamline for all SAXS analyses. LLC samples were sealed in alodined aluminum, hermetic DSC pans (TA Instruments, New Castle, DE) to avoid water loss during analyses. Samples were heated to a desired temperature using a Linkam hot-stage and thermally equilibrated for at least 5 min, prior to X-ray exposure. 2D-SAXS patterns were collected on a Pilatus 2 M detector (25.4 cm × 29.0 cm area with 172 $\mu$m × 172 $\mu$m pixels) upon sample exposure to X-rays for ≤0.1 s. The sample-to-detector distance was calibrated using a silver behenate standard sample ($d$ = 58.38 Å). 2D-SAXS patterns were azimuthally integrated to generate 1D intensity $I(q)$ versus scattering wavevector $q$ (Å$^{-1}$) patterns using the DataSqueeze software package (http://www.physics.upenn.edu/~heiney/datasqueeze/index.html) or using MATLAB-based tools available to users at the 12-ID-B beamline.

## RESULTS AND ANALYSIS

**LLC Self-Assembly of Binary TMA-7*x*/$H_2O$ Mixtures.** We synthesized a homologous series of gemini dicarboxylate surfactants based on decanoic acid with tetramethylammonium counterions (Scheme 1) in high analytical purities following

**Scheme 1. Synthesis of Gemini Didecanoate Surfactants**

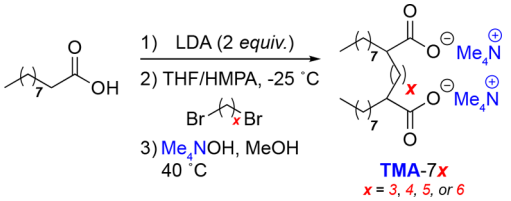


previously described procedures.[54,55] We refer to these surfactants using the nomenclature **TMA-7*x***, where TMA refers to the $NMe_4^+$ counterion, 7 is the number of methylene units in the surfactant tails, and ***x*** is the number of methylene units in the surfactant linker. Sorenson et al.[54] previously determined that **TMA-74** forms aqueous LLC $G_I$ phases over a relatively wide composition window spanning ∼15 wt % surfactant. More recently, Jennings et al.[58] described the aqueous LLC phase behavior of the surfactant **TMA-83u**, which derives from dimerization of 10-undecenoic acid using a $-(CH_2)_3-$ linker, and observed $G_I$ phases that are thermally stable between $T$ = 22 and 100 °C over a 40 wt % wide


https://dx.doi.org/10.1021/acs.langmuir.9b03408
Langmuir 2020, 36, 2307−2321

composition window. Given the sensitivity of the phase behavior of these binary surfactant−water systems to subtle changes in molecular structure, we first sought to map the lyotropic phase behaviors of the homologous series of surfactants **TMA-73**, **TMA-74**, **TMA-75**, and **TMA-76** using high-resolution synchrotron SAXS, as control experiments for subsequent additive studies. While the two aforementioned studies[54,58] reported temperature versus composition phase diagrams in which the composition was specified as a surfactant weight fraction, we instead use headgroup hydration number $w_0$ = (moles $H_2O$)/(moles $-CO_2^-$) as a measure of composition in this work. Since previous work by Perroni et al.[55] demonstrated that gemini dicarboxylate surfactant phase behavior depends sensitively on linker length parity, we structure the description of our findings to focus first on even carbon-linked gemini dicarboxylates and their phase behaviors upon oil loading, before discussing analogous studies with gemini dicarboxylate surfactants bearing odd carbon linkers.

**Aqueous LLCs of Neat Gemini Dicarboxylates with Even Carbon Linkers.** Using synchrotron SAXS, we probed the LLC phase behaviors of pure **TMA-74** and **TMA-76** over the headgroup hydration range $w_0$ = 1.5−38 with $T$ = 22 and 100 °C (Figure 1). SAXS analyses reveal that hydrating **TMA-74** with water in the range $w_0$ = 3−7 at 22 °C results in the formation of stiff, optically nonbirefringent LLCs that exhibit SAXS peaks located at scattering wavevector ratios $(q/q^*)^2$ = 6, 8, 14, 16, 20, 22, *etc.*, consistent with the *Ia3(−)d* space group symmetry of the double gyroid (G) network phase. At $w_0$ = 5, the value of $|q^*|$ = 0.0965 Å$^{-1}$ corresponds to a gyroid cubic unit cell parameter $a$ = 6.51 nm. The observation of 15 resolution-limited SAXS peaks implies the formation of a well-ordered supramolecular assembly with large grain sizes over the entire temperature range. Increasing the water content in these LLCs to 8 ≤ $w_0$ ≤ 33 drives formation of qualitatively softer, optically birefringent mesophases with SAXS peaks located at $(q/q^*)^2$ = 1, 3, 4, 7, 9, *etc.*, at temperatures up to 100 °C (Figure 1). These peak positions correspond to a 2D-hexagonally packed cylinders (H) morphology with *p6mm* symmetry. For the H phase formed at $w_0$ = 10, the $|q^*|$ = 0.213 Å$^{-1}$ corresponds to an intercylinder center-to-center distance of 3.41 nm. When $w_0$ ≥ 34, **TMA-74**/water mixtures form fluid solutions with broad SAXS signatures indicative of concentrated micellar solutions (Iso) that lack translational order. As a result of the phase progression of G → H → Iso with increasing water content, we assign these phases as normal or Type I LLCs in which the interfaces curve toward the hydrophobic domains. The LLC phase behavior of **TMA-74** is summarized in Figure 2A. This phase map concurs with that of Sorenson et al., including the vertical phase boundaries indicative of nearly temperature-invariant phase behavior of these self-assembled surfactant LLCs. Although Gibbs' phase rule predicts regions of two-phase coexistence between the pure phases in this binary phase diagram, no such windows are observed. We ascribe this last observation to the experimental resolution of our phase map, in which $\Delta w_0$ = 2 and $\Delta T$ = 20 °C.

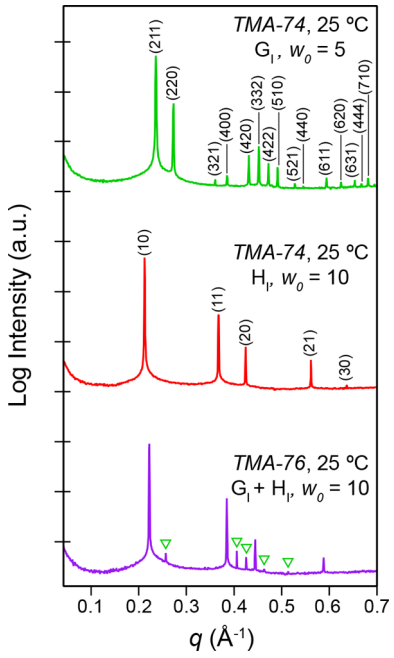


**Figure 1.** Azimuthally integrated 1D-SAXS intensity $I(q)$ versus scattering wavevector $q$ profiles for **TMA-74** and **TMA-76**, indicating the formation of a $G_I$ phase, a $H_I$ phase, and coexisting $G_I$ and $H_I$ phases (markers correspond to the (220), (420), (332), (510), and (440) reflections of the $G_I$ mesophase).

Increasing the surfactant linker length by two methylene units as in **TMA-76** yields a qualitatively similar sequence of Type I LLCs, with a few key differences. At low hydrations $w_0$ = 1.5−2, we observe pronounced wide-angle X-ray peaks indicative of the crystalline surfactant lamellae ($L_\beta$) superposed on a single, broad, and intense scattering feature. Heating this sample to 60 °C drives thermoreversible melting of the $L_\beta$ phase and formation of a LLC lamellar ($L_\alpha$) phase that coexists with a broad scattering feature (see Figure S1). At $w_0$ = 3, **TMA-76** forms a homogeneous viscous dispersion that exhibits the same single broad, high-intensity scattering peak ($q^*$ = 0.2597 Å$^{-1}$). Polarized light microscopy (PLM) analysis reveals that this sample is optically nonbirefringent. These properties are consistent with the formation of a sponge ($L_3$) phase, comprising randomly oriented bilayers that form two interpenetrating labyrinths with no long-range translational order, *i.e.* a disorganized lyotropic network phase. Application of shear to samples sandwiched between glass slides does not trigger any observable shear-induced phase transitions to optically birefringent phases; however, Porcar et al.[59] have noted that shear-induced $L_3$ → $L_\alpha$ transitions in ionic surfactant LLCs require high shear rates ($|\dot{\gamma}| \geq 5$ s$^{-1}$). Increasing the LLC phase water content to $w_0$ = 4−9 enables formation of a $G_I$ phase that melts into a $L_3$ phase above $T \approx$ 60−80 °C, depending on the exact composition. LLCs at hydrations $w_0$ = 12−36 yield $H_I$ phases with SAXS-based evidence for an intervening and expected $G_I/H_I$ two-phase coexistence window at $w_0$ = 10 (Figure 1). Further addition of water induces a lyotropic order-to-disorder transition to a concentrated micellar solution (Iso) at a critical $w_0$ = 38. This phase information is summarized in the temperature versus composition diagram shown in Figure 2B.

**Oil-Swollen Gemini Dicarboxylate LLCs with Even-Carbon Linkers.** Having established the aqueous LLC phase behaviors of **TMA-74** and **TMA-76**, we sought to understand the impact of *n*-decane addition on LLC network phase stability. Samples were prepared by first combining *n*-decane with the dried surfactant powder at a specific mass fraction, followed by three cycles of high-speed centrifugation and


https://dx.doi.org/10.1021/acs.langmuir.9b03408
Langmuir 2020, 36, 2307−2321

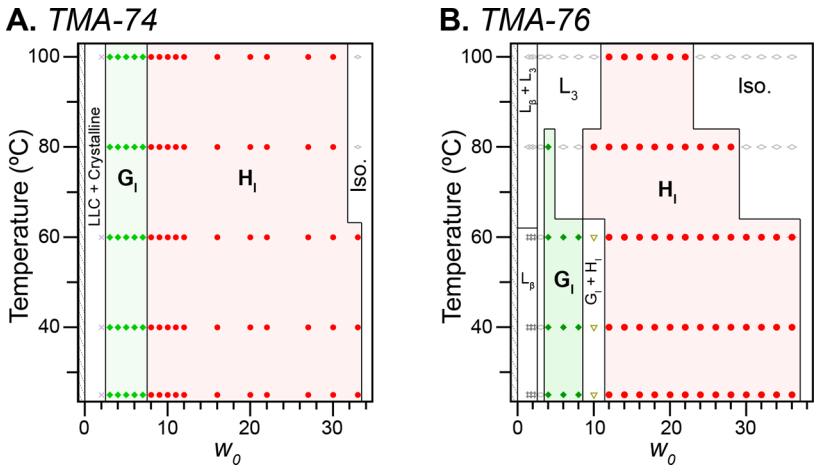


**Figure 2.** Temperature versus surfactant hydration number ($w_0$) aqueous LLC phase diagrams for (A) **TMA-74** and (B) **TMA-76** gemini surfactants, highlighting the influence of hydrocarbon linker length on the stabilities of the observed $G_I$ and $H_I$ LLC phases.

hand-mixing. This surfactant/oil mixture was then hydrated using ultrapure $H_2O$ to achieve the targeted water content or $w_0$-value, followed by a second set of three cycles of centrifugation and hand-mixing to form optically homogeneous LLC samples. These oil-laden LLC phases were then heated to 50 °C for 30 min and allowed to slowly cool to room temperature, followed by resting for 24 h prior to morphological analyses. Heating these samples was crucial to obtaining reproducible results and to maximizing oil loading. All reported phase behavior was determined during the first heating cycle for these samples, unless otherwise noted. To distinguish these samples from the pure **TMA-74** or **TMA-76**, we use the designation **TMA-7*x*_*y*** where $x = 4$ or 6 and $y = 10$ or 40 refers to the weight fraction of *n*-decane (wt %) *relative* to the surfactant mass. In all systems, we found that addition of excess water to these surfactant/oil mixtures yields fluid isotropic, micellar solutions (Iso). Thus, we conclude that all of the observed phases are normal (Type I) morphologies. Addition of 10 wt % *n*-decane to **TMA-74** as in **TMA-74_10** substantially alters the observed LLC phase behavior. While maintaining their thermal stability from $T = 22-100$ °C, the $G_I$ and $H_I$ phase window widths shrink to $w_0 = 3-5$ and $w_0 = 6-16$, respectively. In contrast to pure **TMA-74**, increasing $w_0$ in **TMA-74_10** beyond the $H_I$ phase range leads to a series of complex scattering patterns with relatively broad SAXS peaks (Figure 3).

In a previous report, we demonstrated that *n*-decane swelling of single-tail surfactant tetramethylammonium decanoate (**TMA-Dec**) aqueous LLCs led to the formation of high-curvature micellar C14 and C15 Laves phases ($P6_3/mmc$ and $Fd3(-)m$ space group symmetries, respectively) with large unit cells.[60] On the basis of SAXS patterns reported in that work, we found that **TMA-74_10** LLCs formed in the range $18 \leq w_0 \leq 22$ exhibit two-phase coexistence between $H_I$ and a poorly ordered C15 Laves phase (Figure 3). The breadths of the poorly defined SAXS maxima corresponding to the C15 Laves phases likely stem from its poor translational order. This face-centered cubic C15 phase is a micellar mimic of the $MgCu_2$ intermetallic structure with 24 particles per unit cell and two different classes of oil-swollen micelles situated in an aqueous matrix, which is schematically depicted in Figure 4A. While the C15 phase is well-known in Type II LLCs[61] and is often adjacent to inverse hexagonal ($H_{II}$) assemblies in phase space, Type I C15 phases are rare and have only been observed in

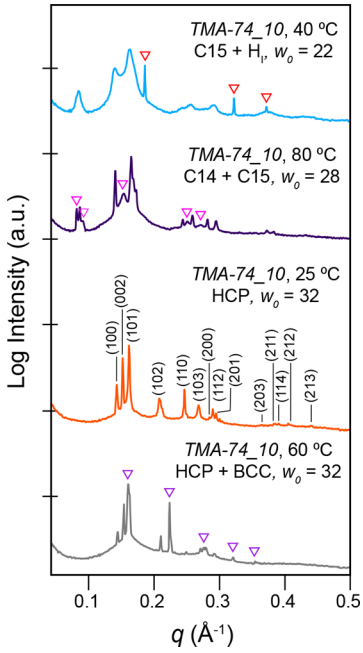


**Figure 3.** 1D-SAXS intensity $I(q)$ versus scattering wavevector $q$ profiles for **TMA-74_10**, indicating C15 + $H_I$ coexistence (markers show the (10), (11), and (20) peaks of $H_I$), C14 + C15 coexistence (markers point to the (100), (101), (103), (213), and (205) peaks of the C14), HCP, and HCP + BCC coexistence (markers indicate the (110), (200), (211), (220), and (310) reflections for BCC).

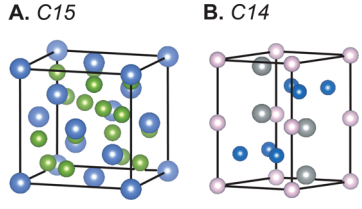


**Figure 4.** Idealized LLC structures for micellar (A) face-centered cubic, C15 Laves phase ($MgCu_2$ intermetallic structure type), and (B) the hexagonal C14 Laves phase ($MgZn_2$ structure).

ternary[60] or quaternary systems.[62] Hydration of **TMA-74_10** to $w_0 = 24-30$ results in complex scattering patterns which we assign as two-phase coexistence between the C15 and C14


https://dx.doi.org/10.1021/acs.langmuir.9b03408
*Langmuir* 2020, 36, 2307−2321

Laves phases (Figure 3), on the basis of our earlier report.[60] The C14 phase, which mirrors the structure of intermetallic alloy $MgZn_2$, comprises a tetrahedral close packing of 12 oil-laden micelles per unit cell of three crystallographically distinct classes with discrete sizes (Figure 4B). Although the C14 Laves phase is of the same crystallographic space group symmetry as hexagonally close-packed spheres (HCP), the larger unit cell dimensions coupled with the unique SAXS peak intensity pattern concur with recent reports of C14 phases in both diblock polymers[63] and LLCs.[60] We note that the samples exhibiting C14/C15 coexistence thermoreversibly transition to C15 + Iso between 80 and 100 °C, suggesting lower stability for the C14 phase at this particular composition. At $w_0$ = 32, the **TMA-74_10** LLCs are soft, optically nonbirefringent solids with sharp SAXS peaks ($|q^*| = 0.124$ Å$^{-1}$) that correspond to a hexagonally close-packed (HCP) spheres morphology with unit cell dimensions $a$ = 5.11 nm and $c$ = 8.29 nm at 25 °C, such that $c/a$ = 1.622 is nearly ideal (Figure 3). Heating this sample leads to coexisting HCP and body-centered cubic (BCC) sphere packings at 60 °C, which ultimately melt into a fluid isotropic state at $T \geq 80$ °C in a manner similar to that reported recently by Jayaraman and Mahanthappa in alkylmalonate single-tail surfactants.[64] The LLC phase behavior of **TMA-74_10** is summarized in Figure 5. While

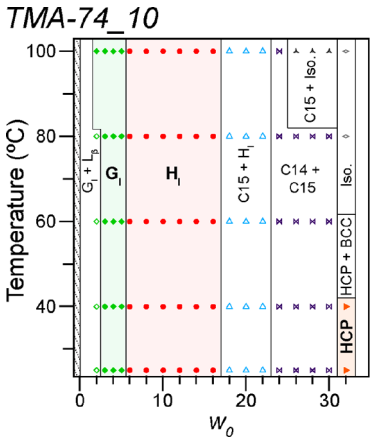


**Figure 5.** Temperature versus surfactant hydration $w_0$ aqueous LLC phase diagram for **TMA-74_10** highlighting the influence of *n*-decane on the stabilities of the observed $G_I$, $H_I$, and micellar LLC phases.

the variety of lyotropic sphere packings in this system may initially seem surprising, our results are entirely consistent with our earlier study of **TMA-Dec** loaded with 40 wt % *n*-decane[60] and related work by Kunieda et al.[57] on two-carbon linked gemini dicarboxylate amphiphiles. The physical origins of these phenomena are considered in the Discussion section (*vide infra*).

Swelling **TMA-74** aqueous LLCs with 40 wt % *n*-decane relative to surfactant leads to an even greater diversity of pure LLC phases, with no signs of oil macrophase separation. **TMA-74_40** samples hydrated to $w_0$ = 3−5 exhibit SAXS patterns with peaks located at $(q/q^*)^2$ = 2, 3, 4, etc., consistent with a cubic, double diamond (D) network phase of four-fold connectors embedded in an aqueous matrix with $Pn3(-)m$ symmetry (Figure 6A). The $|q^*| = 0.1295$ Å$^{-1}$ implies a normal $D_I$ unit cell size of 4.86 nm. While inverse double diamond ($D_{II}$) phases are well-known in monoacylglycerols and other surfactants, the $D_I$ phase is relatively rare and this finding constitutes only the second report of such a phase.[60] Upon increasing the temperature $T \geq 80$ °C in this $w_0$ range, we observe coexisting $D_I$ and $G_I$ network LLC phases (Figure 6B). From $w_0$ = 6−16, **TMA-74_40** self-assembles into optically birefringent $H_I$ LLCs that remain thermally stable to 100 °C. At the slightly higher hydration of $w_0$ = 18−20, the as-prepared sample forms coexisting $H_I$ + C15 phases that heat into a stiff, nonbirefringent material at 100 °C with at least 12 scattering peaks with $(q/q^*)^2$ = 3, 8, 11, 12, ... of a pure C15 Laves phase ($a$ = 12.54 nm; Figure 6A). While we observe C14/C15 phase coexistence in the range $w_0$ = 22−26, heating these samples leads to either a pure C15 phase or C15 + Iso, again suggesting that the C14 phase is slightly less stable than the C15 phase. Micellar HCP packings are again observed at the relatively high hydrations $w_0$ = 28−38, with composition-dependent thermal stabilities. Heating the initially formed HCP sample at $w_0$ = 28 formed by **TMA-74_40** leads to HCP/C15 coexistence at 40 °C (Figure 6B) and a new HCP/C15/C14 three-phase coexistence at 60 °C (Figure 6B). While such phase coexistence is uncommon, it is allowed by Gibbs' phase rule for this three-component microemulsion system. Further heating of this sample to 80 °C leads to C14/C15 coexistence followed by an order−disorder transition (ODT) at 100 °C (Figure S2). Upon slow cooling to room temperature, we obtain an stiff, optically nonbirefringent LLC phase with approximately 30 scattering peaks ($a$ = 9.28 nm; $c/a$ = 1.633) corresponding to the distinctive scattering signature associated with a pure C14 Laves LLC phase (Figure 7; see Figure S3 for a fully indexed SAXS pattern and Table S1 for a list of SAXS peak positions and residuals). This result constitutes only the second report of this complex micellar LLC morphology.[60] The fact that we do not observe a pure C14 phase upon SAXS analysis of the as-made sample, coupled with the sequence of order-to-order transitions between various spherical micelle packings, suggests that the free energy differences between these phases are small. Consequently, the observed LLC morphology depends sensitively on the kinetics of phase nucleation and growth that are controlled by thermal processing conditions per recent reports.[63,64] At the highest water content, $w_0$ = 40−42, self-assembly into soft, nonbirefringent LLCs consistent with body-centered cubic (BCC) spheres $(q/q^*)^2$ = 2, 4, 6, etc.; Figure 6A) is observed. The $|q^*|$ = 0.1060 value for this micellar ensemble indicates a unit cell of 5.95 nm. This material transforms into fluid isotropic micelles at $T \geq 60$ °C. The phase behavior of **TMA-74_40** is summarized in Figure 8A. We note that the aqueous LLC phase behaviors of **TMA-74_20** and **TMA-74_30** at 25 °C (20 and 30 wt % *n*-decane relative to surfactant, respectively) will be discussed later in the context of an isothermal ternary phase portrait.

**TMA-76_40** LLCs comprising 40 wt % *n*-decane (Figure 8B) relative to **TMA-76** display qualitatively similar phase behavior changes as compared to **TMA-74_40** and **TMA-74**. At low hydrations, we observe $L_\beta$ and $D_I$ phase coexistence in **TMA-76_40** ($w_0 < 2$) and $L_3$ sponge phase formation when $w_0$ = 2−3. Upon increasing LLC hydration across the range $w_0$ = 4−8, the $D_I$ and $G_I$ network phases remain thermally stable up to 60 °C. $H_I$ LLCs form over a wide phase window spanning $w_0$ = 10−22, which give way to the phase sequence $H_I$/C15/C14 → C14 → C14/C15/HCP → C14 + C15 → HCP → BCC → Iso over the range $w_0$ = 24−44 at 22 °C (see Figure 8B). Different from the case of **TMA-74_40** at $w_0$ = 28, a pure C14 phase is observed to form in the as-prepared sample at $w_0$


https://dx.doi.org/10.1021/acs.langmuir.9b03408
Langmuir 2020, 36, 2307−2321

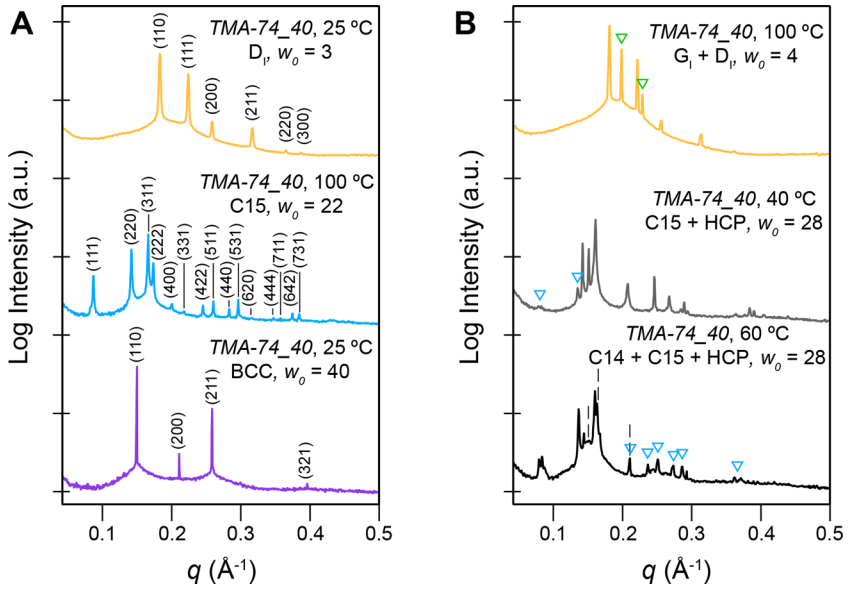


**Figure 6.** Azimuthally integrated 1D-SAXS intensity $I(q)$ versus scattering wavevector $q$ profiles for **TMA-74_40**, indicating (A) pure $D_I$, C15, and BCC mesophases and (B) $D_I$ + $G_I$ (markers indicate the (211) and (220) peaks of the $G_I$ morphology), HCP + C15 (markers point to the (111) and (220) peaks of the C15), and HCP + C14 + C15 (dashed lines highlight the (002), (101), and (102) peaks of the HCP phase; markers show the (331), (422), (511), (440), (531), and (642) reflections for C15) morphologies.

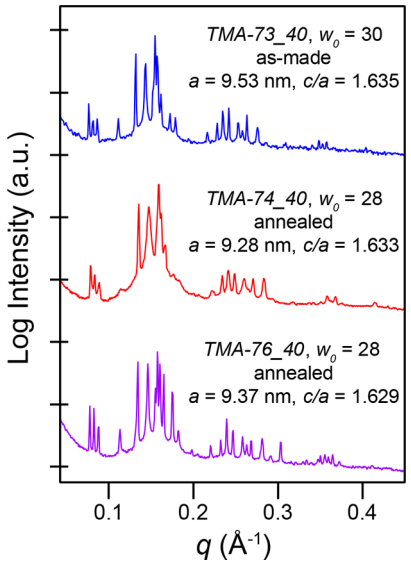


**Figure 7.** Azimuthally integrated 1D-SAXS intensity $I(q)$ versus scattering wavevector $q$ profiles for **TMA-73_40**, **TMA-74_40**, and **TMA-76_40**, highlighting the large number of peaks, which characterize the exceptionally well-ordered C14 Laves phases stabilized in each of these *n*-decane swollen aqueous LLC phases.

= 28 prior to any thermal annealing. However, we note that heating above the ODT temperature $T_{ODT} \approx 60$ °C and slow cooling from the disordered micellar "melt" results in the very well-defined pattern with at least 32 SAXS maxima presented in Figure 7.

**Pure Gemini Dicarboxylates with Odd-Carbon Linkers.** We next used synchrotron SAXS to probe the LLC phase behaviors of neat **TMA-73** and **TMA-75** surfactants (no oil) with headgroup hydrations $w_0$ = 2−44 between $T$ = 22−100 °C. For **TMA-73** surfactants, $G_I$ phases form when $4 \leq w_0 \leq 13$ with composition-dependent thermal stabilities. For the LLC assembly formed with $w_0$ = 13, heating above 80 °C leads to an order−order transition from $G_I$ to $H_I$. A large $H_I$ phase window is observed between $w_0$ = 16−30. These samples exhibit $T_{ODT} \geq 60$ °C, the ODT temperature of which depends on the surfactant composition. Hydrating this binary mixture above $w_0$ = 32 yields fluid isotropic micellar solutions. This morphological behavior is compiled in the phase diagram given in Figure 9A. When the odd-carbon linker is extended to contain five methylene units ($-(CH_2)_5-$), as in **TMA-75**, we do not document significant changes in the LLC phase behavior as compared to **TMA-73** (Figure 9B). The $-(CH_2)_5-$ linker apparently leads to lower surfactant crystallinity than **TMA-73**, which drives $G_I$ + $L_\beta$ phase coexistence at headgroup hydrations as low as $w_0$ = 2. As water content is increased to $w_0$ = 4−14, the $G_I$ LLC network is stabilized up to $T$ = 100 °C, except at $w_0$ = 14, where we observe a transition to a $H_I$ phase above 40 °C. This $H_I$ phase window extends up to $w_0$ = 46, with decreasing thermal stability as $w_0$ increases.

**Oil-Swollen Gemini Dicarboxylate LLCs with Odd-Carbon Linkers.** Having assessed the binary LLC phase behaviors of **TMA-73** and **TMA-75**, we turn our attention now to their ternary phase behaviors upon *n*-decane addition. Addition of 10 wt % *n*-decane to **TMA-73**, as in **TMA-73_10**, only marginally alters the $G_I$ and $H_I$ phase stabilities as summarized in the phase diagram given in Figure 10. More specifically, the $G_I$ phase window shifts to lower $w_0$ = 2−10 with no perceptible change in the window width at the resolution of our phase map ($\Delta w_0$ = 2). The $H_I$ phase window spans $w_0$ = 12−24 at 22 °C. At $w_0$ = 24, we observe an order−order phase transition from $H_I$ to $H_I$/C15 coexistence near 80 °C, followed by melting into a micellar fluid at 100 °C. Hydration to $w_0$ = 26 yields $H_I$/C14/C15 three-phase coexistence, which transforms into C14/C15 micellar phase coexistence at 80 °C. We observe a pure C14 phase at $w_0$ = 30 in the as-made LLC sample (Figure S4), which is thermally stable up to 60 °C. Micellar HCP packings are formed at ambient temperature at the higher hydrations of $w_0$ = 32−34, and these phases undergo order−order transitions to BCC


https://dx.doi.org/10.1021/acs.langmuir.9b03408
Langmuir 2020, 36, 2307−2321

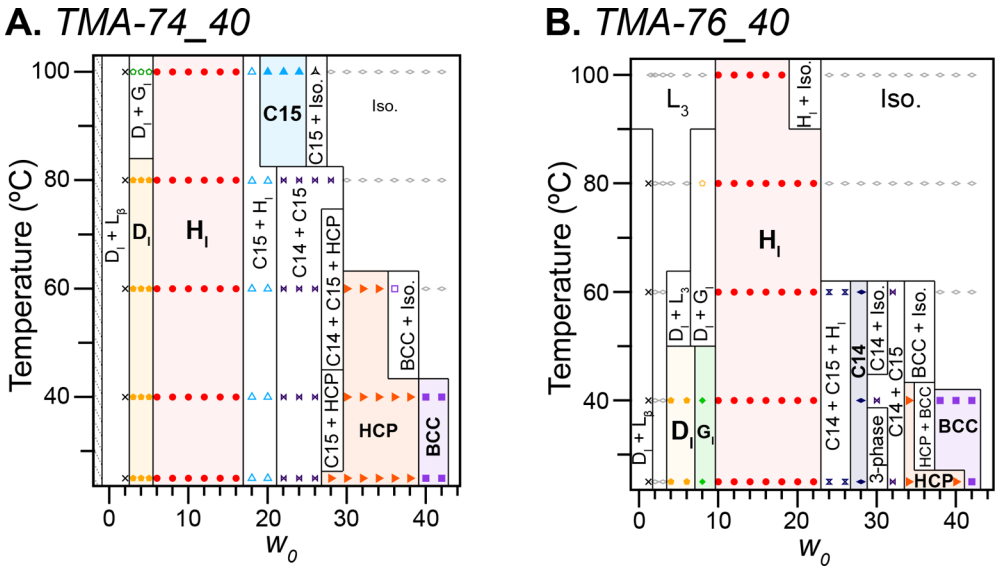


**Figure 8.** Temperature versus surfactant hydration $w_0$ aqueous LLC phase diagrams with 40 wt % *n*-decane added on heating for (A) **TMA-74_40** and (B) **TMA-76_40** gemini surfactants highlighting the influence of hydrocarbon linker length on the stabilities of the observed network, $H_I$, and micellar LLCs.

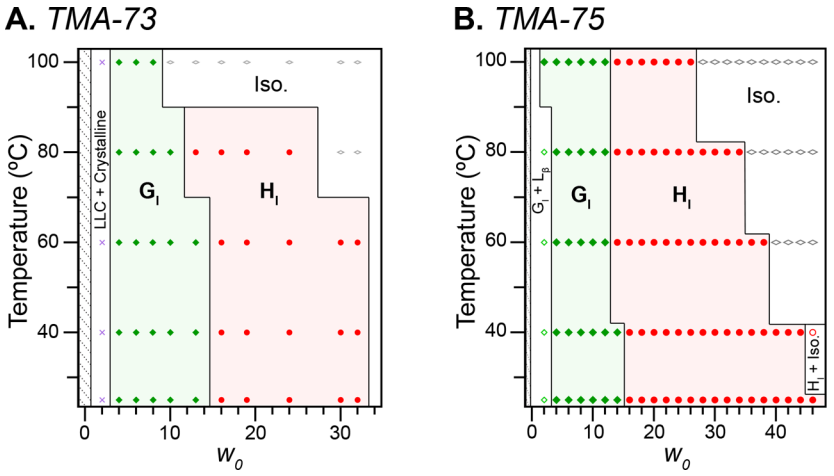


**Figure 9.** Temperature versus surfactant hydration $w_0$ aqueous LLC phase diagrams for (A) **TMA-73** and (B) **TMA-75** gemini surfactants highlighting the influence of hydrocarbon linker length on the stabilities of the observed $G_I$ and $H_I$ LLCs.

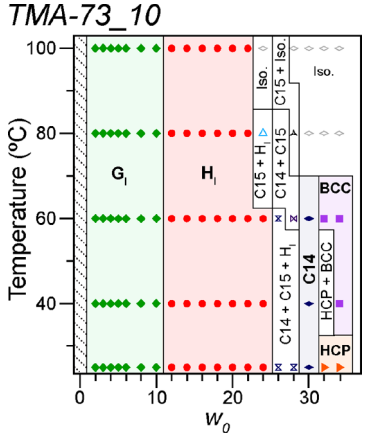


**Figure 10.** Temperature versus surfactant hydration $w_0$ aqueous LLC phase diagrams for **TMA-73_10** gemini surfactants highlighting the influence of *n*-decane on the stabilities of the observed $G_I$, $H_I$, and micellar LLCs.

phases at $T \approx 60$ °C that give way to fluid isotropic (Iso) micellar solutions at $T > 60$ °C.

Increasing the *n*-decane loading to 40 wt % in **TMA-73_40** does not substantially change the phase diagram (Figure 11A) as compared to **TMA-73_10** (Figure 10), with two significant exceptions. The network phase window remarkably retains its width, yet it bifurcates into pure $D_I$ ($w_0 = 2-6$) and $G_I$ ($w_0 = 8-10$) phases. While the $H_I$ phase window remains largely unchanged in the headgroup hydration range $12 \leq w_0 \leq 24$, we note that this phase is only birefringent in the range $w_0 = 12-20$. When the surfactant headgroup hydration number $w_0 = 22-24$, SAXS analyses of the LLCs yields patterns that appear to have *p6mm* symmetry with peaks located at $(q/q^*)^2 = 1$, 3, 4, 7, and 9. However, these samples are optically non-birefringent and their physical textures are notably softer than the birefringent $H_I$ phase. The lack of optical birefringence suggests one of two possibilities: (1) that the phase is refractive index contrast-matched such that no birefringence is recorded or (2) that this phase is a new packing of spherical micelles that exhibits no detectable birefringence. Given that the former


https://dx.doi.org/10.1021/acs.langmuir.9b03408
Langmuir 2020, 36, 2307−2321

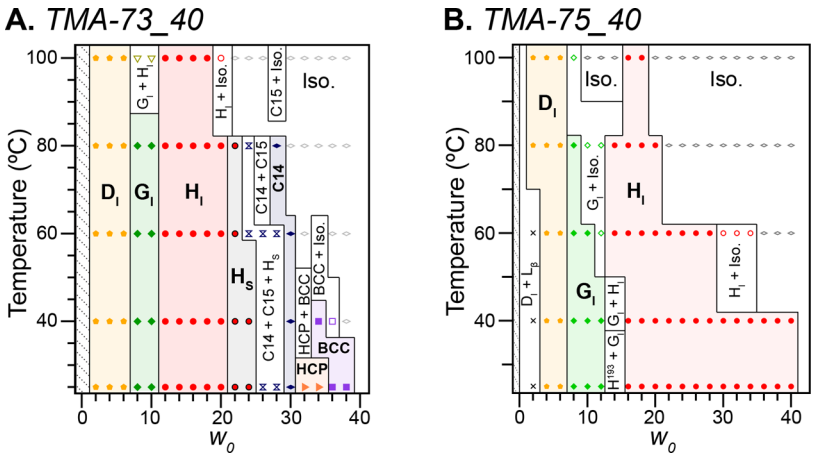


**Figure 11.** Temperature versus surfactant hydration $w_0$ aqueous LLC phase diagrams for (A) **TMA-73_40** and (B) **TMA-75_40** gemini surfactants highlighting the influence of hydrocarbon linker length on the stabilities of the observed network, $H_I$, and micellar LLCs.

notion is likely not true, the symmetry deduced from the SAXS data suggests the packing of spherical micelles into a simple hexagonal phase that we designate $H_S$. Note that a similar $H_S$ phase with *P6mmm* symmetry was recently reported by Zhang et al. in self-assembling poly(styrene-*block*-poly(4,1-isoprene)-*block*-styrene-*block*-ethylene oxide) tetrablock terpolymers.[65] At higher hydrations of $w_0 \geq 26$, we observe other discrete micellar LLCs as either coexisting or pure phases. Note that both **TMA-73_10** and **TMA-73_40** form pure C14 phases at $w_0 = 28$ (Figures S4 and 7, respectively), and they both form HCP at $w_0 = 32-34$. BCC LLCs are formed at the highest water contents of $w_0 = 36-38$, above which we observe a lyotropic order−disorder transition to isotropic micellar solutions.

While the addition of oil apparently fosters formation of micellar morphologies in the systems discussed thus far, **TMA-75_40** surprisingly shows no such morphologies upon the addition of 40 wt % *n*-decane (Figure 11B). However, oil addition again triggers bifurcation of the network phase window located between $2 < w_0 < 14$ into regions of pure $D_I$ and $G_I$ phases. At $w_0 = 14$, we observe coexistence of lyotropic $G_I$ and the 3D-hexagonal network $H_I^{193}$ phases with space group symmetry $P6_3/mcm$ (see Figure S5 for indexed SAXS pattern).[56] This coexistence is well-precedented in other systems and is expected, since the theoretically anticipated mean curvature of the $H_I^{193}$ phase is between that of $G_I$ and $H_I$ morphologies as previously noted.[22,56,66] Heating this sample to 40 °C leads to $G_I/H_I$ coexistence, which transforms to pure $H_I$ at 60 °C, and it finally disorders at 100 °C. This phase sequence on heating is reminiscent of that previously documented for the disodium gemini dicarboxylate **Na-94**, derived from dimerization of dodecanoic acid with a $-(CH_2)_4-$ linker.[56] At the highest hydrations ($w_0 = 16-40$), **TMA-75_40** forms hexagonally-packed cylinders. Only freely flowing micellar solutions are observed for $w_0 > 40$ with the notable absence of any ordered spherical micelle packings.

In order to facilitate visualization and comparisons of the phase behaviors of *n*-decane swollen **TMA-74** and **TMA-73**, we recast the morphology data for the as-made samples at 22 °C (presented in Figures 2A, 5, and 8A, and 9A, 10, and 11A, respectively) as ternary phase diagrams per the convention in the surfactant/oil/water microemulsion literature. Note that we have included the results of phase mapping studies for *n*-decane loadings of 20 and 30 wt % relative to surfactant mass for each of these amphiphiles at 22 °C, in order to clarify how the phase windows evolve upon oil addition. Since the axes of these ternary phase diagrams are net weight fractions, a constant *n*-decane loading relative to surfactant mass corresponds to a systematically varied *n*-decane content as a function of water weight fraction. In other words, each data series derived from a single *n*-decane loading level is not an isopleth. The ternary phase diagram for **TMA-74** reveals that its phase behavior is altered by the addition of *n*-decane (Figure 12A). While addition of <20 wt % oil to **TMA-74**

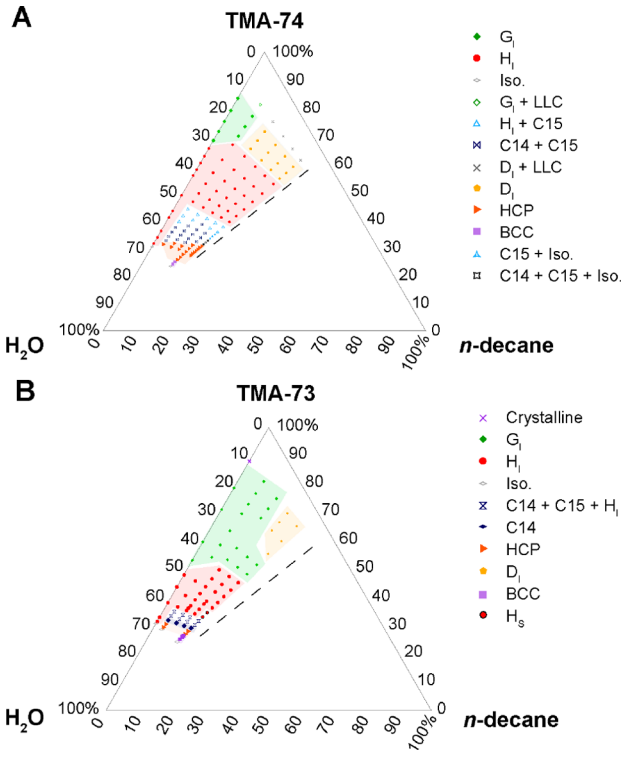


**Figure 12.** Ternary LLC phase diagrams of surfactant:water:*n*-decane at 22 °C for (A) **TMA-74** and (B) **TMA-73** gemini surfactants highlighting the effect of hydrocarbon linker length on the stabilities of the observed network, $H_I$, and micellar LLCs. The dashed line demarcates the limit where these microemulsion systems undergo visible *n*-decane macrophase separation.


https://dx.doi.org/10.1021/acs.langmuir.9b03408
*Langmuir* 2020, 36, 2307−2321

LLCs does not appreciably diminish the width of the network phase window including $D_I$, $G_I$, and $D_I/G_I$ phase coexistence (range of $w_0$ values spanning $\Delta w_0 = 3$; see Figure S6), the addition of ≥20 wt % *n*-decane relative to the surfactant mass triggers complete transformation of the $G_I$ phases into $D_I$ phases. At higher headgroup hydrations, as little as 10 wt % *n*-decane loading drives the formation of a plethora of micellar packings, some of which become more well-ordered at high oil loadings as in the case of the C14 phases (Figure 7).

On the other hand, the phase behavior of **TMA-73** is less strongly perturbed by the addition of *n*-decane (Figure 12B). For example, pure $G_I$ phases form at low water contents with *n*-decane loadings as high as 20 wt %. Beyond this oil loading, this $G_I$ phase window bifurcates into $D_I$ and $G_I$ phase windows. However, the overall width of the LLC network phase window remains wide ($\Delta w_0 = 9$; see Figure S6) with only a marginal decrease relative to the binary **TMA-73**/$H_2O$ LLC system. Similarly, the **TMA-73** $H_I$ phase is more tolerant to oil addition and a relatively narrow window of spherical micelle packings is observed at high hydration, as compared to **TMA-74**. In spite of these differences in the phase behaviors of **TMA-74** and **TMA-73** aqueous LLCs loaded with *n*-decane, we note that both surfactants accommodate up to 35 wt % *n*-decane in total prior to the onset of oil macrophase separation. Consistent with this observation, Jennings et al.[58] observed that LLCs of the related surfactant **TMA-83u** are able to incorporate up to 37 wt % of the hydrophobic HDDMA monomer. A remarkable feature of the four gemini surfactants used in this study is that the $N_I$ phase stability exhibited in the binary **TMA-7*x***/$H_2O$ system is reflected in their ternary, oil-loaded LLC mesophases. More quantitatively, the network window hydration range $\Delta w_0$ for the binary LLCs decreases in the order:

$$\textbf{TMA-75}\ (\Delta w_0 = 13) > \textbf{TMA-73}\ (\Delta w_0 = 10) > \textbf{TMA-74}\ (\Delta w_0 = 5) = \textbf{TMA-76}\ (\Delta w_0 = 5)$$

This ordering is reminiscent of an earlier report by Perroni et al.,[55] in which a similar trend was demonstrated for **Na-7*x*** and **K-7*x*** ($x$ = 3, 4, and 5) gemini didecanoate surfactants bearing either $Na^+$ or $K^+$ counterions in the absence of oil. Oil loading of the amphiphile LLCs with TMA counterions preserves this linker length parity trend ("odd/even effect"), with only modest decreases in the network window widths upon addition of 10 or 40 wt % *n*-decane.

Incorporation of *n*-decane into **TMA-73** and **TMA-74** LLC phases also impacts the preferred domain spacings ($d$) of their self-assembled morphologies. Figure 13 depicts the observed domain spacings for the $D_I$, $G_I$, and $H_I$ phases of **TMA-73** and **TMA-74** deduced from SAXS analyses at various weight percent oil loadings. In the case of the $H_I$ and $G_I$ phases, we find that the observed LLC $d$-spacings increase with water content ($w_0$) in both the neat surfactant LLCs and upon oil swelling. This effect probably stems from the lateral expansion of the hydrophilic domains due to increased water volume fraction.

The addition of hydrocarbon oil dilates the observed $G_I$ and $H_I$ phase $d$-spacings by ~11% relative to the binary **TMA-7*x*** ($x$ = 3 or 4) aqueous LLCs; somewhat surprisingly, the unit cell parameters apparently do not change appreciably on increasing the oil loading level from 10 to 40 wt % relative to the surfactant mass. However, the $d$-spacings for the $D_I$ phase apparently decrease by ~10% with increasing LLC water content and their absolute values appear to be invariant with oil loading level at similar hydrations. X-ray analyses of these $D_I$ phases indicate that the SAXS peak intensities change appreciably with water content, suggesting that the cables of the double diamond phase thin upon increased hydration in a manner consistent with an increased interfacial per surfactant on water addition at low hydrations.

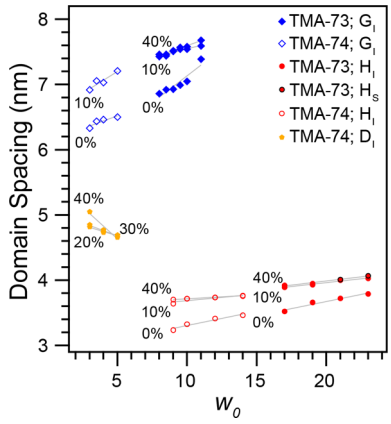


**Figure 13.** Domain spacing versus $w_0$ for **TMA-74** and **TMA-73** surfactants, demonstrating the effect of different *n*-decane loadings (relative to surfactant weight) on the $D_I$, $G_I$, and $H_I$ LLC unit cell dimensions at fixed water contents.

## DISCUSSION

While the aqueous LLC phase behaviors of ionic single-tail amphiphiles are readily rationalized in terms of the relative volumes filled by the hydrated counterion−headgroup pair and the hydrophobic tail due to the average axial symmetry of these molecules along the tail end-to-headgroup vector, the self-assembly behavior of gemini didecanoate amphiphiles is much more complex. Recent molecular dynamics (MD) simulations by Mondal et al.[67] indicate that the phase behaviors of these architecturally complex dicarboxylate surfactants stem from their unique conformational preferences on hydration that induce their frustrated interfacial packings. For gemini dicarboxylates **M-74** (M = $Na^+$, $K^+$, or $TMA^+$), MD simulations reveal that amphiphile hydration enforces restricted conformations that minimize water-hydrophobe contacts while maximizing ionic counterion-headgroup solvation. Figure 14A schematically depicts the splayed tail

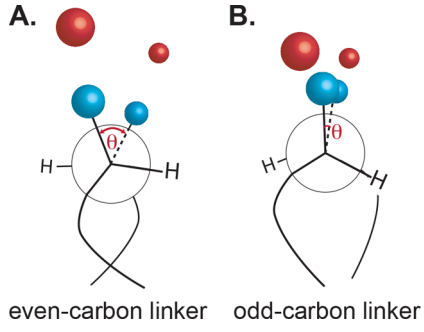


**Figure 14.** Pseudo-Newman projections of **TMA-7*x*** surfactant conformations along the linker axis demonstrating differences in the relative headgroup orientations and degrees of tail splay specified by (A) even and (B) odd linkers, which impact the relative levels of counterion dissociation.


https://dx.doi.org/10.1021/acs.langmuir.9b03408
Langmuir 2020, 36, 2307−2321

molecular conformation of a hydrated **M-74** amphiphile in a $G_I$ LLC, wherein an average interheadgroup dihedral angle $\langle\theta\rangle \approx 55-60°$ mitigates intermolecular Coulombic repulsions between the headgroups by increasing the distance between them. Since supramolecular packing of this anisotropic surfactant conformation into zero curvature $L_\alpha$ phases incurs energetically costly contacts between water and the splayed hydrophobic tails upon counterion dissociation at modest hydrations ($w_0$), the unstable $L_\alpha$ bilayers wrinkle to shield the tails from unfavorable water contacts. Consequently, $G_I$ phases with negative Gaussian ("saddle splay") curvature form over wide temperature and LLC composition (up to 20 wt % wide) windows. On this basis, the high degree of tetramethylammonium carboxylate ion pair dissociation in **TMA-74** even at low hydrations explains the complete destabilization of the $L_\alpha$ phase in favor of the $G_I$ morphology at low $w_0$. Thus, this model serves to explain why **TMA-74** and **TMA-76** do not form $L_\alpha$ phases in favor of $G_I$ phases with modest widths, which give way to $H_I$ phases at higher hydrations.

Detailed MD simulations by Mantha et al.[68] addressed the origins of the experimental observations by Perroni et al. that odd-carbon linkers even further stabilize **Na-73** and **Na-75** $G_I$ phases. Atomistic MD studies demonstrate that these hydrated surfactants exhibit different conformational preferences as compared to their **Na-74** and **Na-76** homologues with even carbon linkers: the splay angles between the headgroups are much smaller (≤15°; see Figure 14B) and are nearly invariant with headgroup hydration $w_0$ for the odd-carbon linked amphiphiles due to preferred linker conformations. Consequently, proximity of adjacent headgroups disallows the high degrees of counterion dissociation observed in even-carbon linked surfactants. Thus, interfacial localization of the $TMA^+$ counterions stabilizes relatively low mean curvature $G_I$ phases and restricts $H_I$ phase formation to smaller hydration windows. In other words, the wide $G_I$ phase windows of gemini didecanoates generally derive from destabilization of the adjacent $L_\alpha$ and $H_I$ phases. Mantha et al.[68] noted that different degrees of counterion-headgroup dissociation may impact the electrostatic energy balance between the observed phases, such that more dissociated counterions such as $TMA^+$ may completely destabilize the $L_\alpha$ phase at low hydrations while enabling $H_I$ formation only at high $w_0$ as experimentally observed in **TMA-73** and **TMA-75** LLCs (Figure 9).

The self-assembly of *n*-decane/$H_2O$/**TMA-7*x*** ($x$ = 3, 4, 5, and 6) ternary LLC mesophases mirrors this dichotomous phase behavior, such that odd-carbon linked surfactants stabilize network LLC phases ($G_I$ and $D_I$) while even-carbon linked surfactants adopt higher mean interfacial curvature phases (e.g., micelle packings) at the expense of reduced $G_I$ and $H_I$ phase stabilities. The formation of micellar LLCs in oil-loaded **TMA-74** and **TMA-76** may be understood by considering the impact of adding a pure hydrocarbon oil, which segregates strongly toward the hydrophobic domain centers. Oil segregation to the core of a cylindrical micelle in a $H_I$ phase reduces the interfacial curvature of the aggregate, resulting in reduced surfactant intermolecular distances that incur additional Coulombic repulsions between the surfactant headgroups. One means of relieving this electrostatic strain and maintaining the same interfacial area per surfactant as prior to oil addition is for the cylindrical micelles to pinch off and form oil-swollen spherical micelles (Figure 15). Kunieda and co-workers have demonstrated exactly this effect in both nonionic and ionic surfactant aqueous LLCs.[57,69] In oil-swollen **TMA-73**

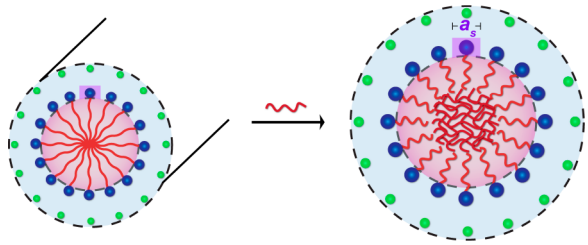


**Figure 15.** Schematic depiction of the impact of oil swelling of the hydrophobic domains of a $H_I$ morphology, illustrating how preservation of the $w_0$-dictated interfacial area per surfactant ($a_S$ in *purple*) upon *n*-decane addition requires the cylindrical micelles to pinch off to form spherical, oil-loaded micelles

and **TMA-75** LLCs, the highly correlated counterion distributions lead to reduced interfacial bending rigidity so that these supramolecular assemblies shelter large amounts of oil within their hydrophobic domains without appreciably changing the headgroup hydration range ($\Delta w_0$) over which $G_I$ and $H_I$ phases form. The physical phenomena underlying the formation of spherical micelle packings by oil-loaded **TMA-73** and the absence of such behavior in **TMA-75** are currently unknown and are the subject of ongoing investigations.

While prior work on ionic gemini surfactant LLC self-assembly has suggested that the only network phases that form are $G_I$ and $H_I$[193] phases built from 3-fold connectors,[56] all of the aqueous **TMA-7*x*** LLCs form $D_I$ phases upon swelling with *n*-decane. A distinguishing characteristic of LLC network phases is that the interfaces of their multivalent connectors exhibit deviations from a constant mean curvature, including regions of zero mean curvature and negative Gaussian curvature. These interfacial curvature variations imply differential headgroup-counterion solvation or differences in tail packing at different points along the domain interfaces, both of which are energetically costly. Thus, network phase selection has previously been rationalized in terms of the minimizing deviations from a constant mean interfacial curvature. Calculations by Matsen and Bates[25] for generic G and D surfaces, and more recent geometric calculations by Chen and Jin[70] on normal network LLCs, suggest that the relative $G_I$ and $D_I$ phase stabilities specifically depend on the hydrophobic volume fraction. More explicitly, the phase that minimizes deviations from a constant mean curvature varies with the hydrophobic volume fraction, such that the $D_I$ phase is thermodynamically more stable at higher hydrophobic volume fractions than the $G_I$ phase. Thus, addition of a critical amount of *n*-decane to a $G_I$ LLC increases the net hydrophobic volume fraction of the assembly enough to drive $D_I$ phase formation. For example, a **TMA-73** $G_I$ phase at $w_0$ = 6 exhibits a hydrophobic volume fraction of 71 vol %, whereas **TMA-73_40** at the same $w_0$ = 6 forms a $D_I$ phase with net hydrophobic volume fraction 77.4 vol % (assuming equal mass densities of 1 g/cm$^3$ for the hydrocarbon and aqueous domains). However, further addition of water to these oil-swollen $D_I$ phases formed at low $w_0$-values increases the hydrophilic volume fraction, thus stimulating a phase transition to $G_I$ structure.

Near the lyotropic ODT for oil-swollen **TMA-7*x*** ($x$ = 3, 4, and 6) aqueous LLCs, we observe a series of spherical micelle packings, including high symmetry body-centered cubic (BCC) and hexagonally closest-packed (HCP) spheres, as well low symmetry C14, C15, and $H_S$ phases. On decreasing


https://dx.doi.org/10.1021/acs.langmuir.9b03408
Langmuir 2020, 36, 2307−2321

hydration from the fluid isotropic micellar state at high $w_0$, we generally observe the isothermal phase transition sequence BCC → HCP → C14 → C15 → $H_I$, sometimes with intermediate windows of two-phase coexistence. This phase sequence is similar to that of the single-tail surfactant analog **TMA-Dec_40**, in which we first reported the formation of an exceptionally well-ordered C14 Laves phase.[60] By analogy to the argument presented above for network phase selection, the micellar sphere packing phase selection stems from minimization in costly variations in the mean interfacial curvature of the aggregates while maximizing intermicellar cohesion.[60,64,71−73] Upon dehydration of an isotropic micellar solution, the first phase to form is BCC LLCs since the configurational entropy loss upon crystallization is minimized in this phase due to the symmetry equivalence of all lattice sites.[74] As $w_0$ decreases further, the counterion clouds around the micelles distort to conform to the Wigner−Seitz (W−S) cells or Voronoi partition of the lattice. That is to say, the electrostatic cohesion among the micelles is maximized by localizing the counterions on planes that perpendicularly bisect the vectors connecting adjacent lattice sites.[73] However, this polyhedral distortion of the micellar counterion clouds implies energetically unfavorable, differential hydration of the surfactant headgroup-counterion pairs. To minimize such deviations (maximize the spherical character of the counterion cloud), the micellar aggregates reconfigure in a manner that increases the overall average coordination number ($\langle CN \rangle$) of each lattice site by redistribution of both oil and surfactant chains. However, the increase in $\langle CN \rangle$ that maximizes the average sphericity of the counterion clouds while also maximizing electrostatic cohesion in the ensemble is necessarily accompanied by a decrease in the global lattice symmetry.[72,73]

The optimal lattices that maximize $\langle CN \rangle$ and micellar cohesion are tetrahedrally close-packed Frank−Kasper (FK) phases.[75,76] The sphericity of a polyhedron may be quantified using the isoperimetric quotient of Polya, defined as $IQ = 36\pi V^2/S^3$, where $V$ and $S$ are the respective polyhedron volume and surface area; $IQ = 1$ for a perfect sphere. FK phase selection in thermotropic liquid crystalline dendrons,[77,78] diblock polymers,[63,72,76] and LLCs[60,64,71,73,79] has been rationalized in terms of the order of decreasing $IQ$ subject to the constraint of minimizing the average interfacial area per surfactant, as in the diblock foam model of Grason and coworkers.[75] The free energies that separate these various phases are likely minute, and thus FK phase selection in the ternary surfactant/oil/water studied here are likely governed by the kinetics of phase nucleation and growth and may not necessarily reflect the thermodynamically preferred equilibrium morphology.[79] One such example is the case of the C14 phase scattering patterns provided in Figure 6, in which the LLC formed by **TMA_74_40** at $w_0 = 28$ initially exhibits a mixture of HCP, C15, and C14 phases. This complex phase coexistence is not unexpected given that the HCP and C14 LLCs exhibit the same $P6_3/mmc$ space group symmetry, and the C14 and C15 ($Fd3(-)m$ symmetry) are structurally related by stacking faults,[80] in a manner similar to the relationship between the simpler HCP and face-centered cubic (FCC) sphere packings. However, heating this sample above its thermotropic ODT and slow cooling to room temperature enables the formation of a pure C14 phase. As noted in recent reports of FK A15, σ, and Laves C14 and C15 LLC phases, the formation of low-symmetry ordered states typically occurs with exceptional long-range translation order indicated by the large number of resolution-limited SAXS peaks.[60,63,64,72,73,79] On this basis, we extracted the Fourier amplitudes associated with each SAXS peak using a Le Bail refinement using the *JANA2006* program[81] and used this information as an input for the charge-flipping algorithm *SUPERFLIP*[82] to reconstruct the electron density map in Figure 16 for the C14 phase formed by

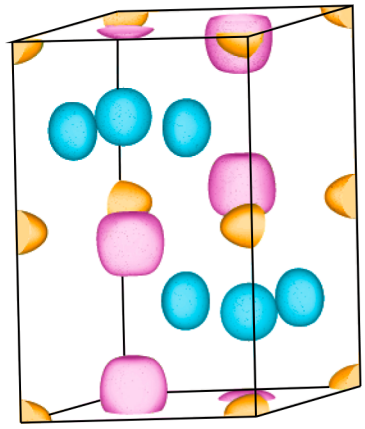

**Figure 16.** 3D electron density map (90% negative isosurface) generated from the experimental C14 Laves LLC phase observed in **TMA-76_40** at a surfactant hydration $w_0 = 28$, indicating three distinct classes of oil-laden micelles located at the 6*h* (blue), 4*f* (pink), and 2*a* (gold) Wyckoff positions of the hexagonal unit cell.

**TMA-76_40** at $w_0 = 28$ (see the Supporting Information for details of this procedure). This electron density map demonstrates faceting of the micelles, the interfaces of which deviate from constant mean curvature, thus reflecting variations in surfactant headgroup-counterion pair hydration across the assembly.

## CONCLUSION

Studies of the aqueous lyotropic phase behaviors of ternary mixtures of *n*-decane/$H_2O$/**TMA-7*x*** gemini dicarboxylate surfactants ($x$ = 3, 4, 5, and 6) with various *n*-decane loadings reveal a sensitive dependence of the self-assembled morphologies on the surfactant linker length. Aqueous LLCs of **TMA-7*x*** surfactants ($x$ = 3 or 5) with odd-carbon linkers exhibit wide normal gyroid ($G_I$) and hexagonally-packed cylinders ($H_I$) phase windows, and the network ($N_I$) phase window width is remarkably well preserved in ternary compositions comprising up to 30 wt % oil albeit with an oil-induced order−order phase transition to a normal double diamond ($D_I$) phase. However, **TMA-7*x*** surfactants ($x$ = 4 or 6) with even-carbon linkers exhibit dichotomous phase behavior: oil addition generally diminishes the composition window width over which $N_I$ phases form, and the addition of oil to the $H_I$ phases results in the formation of low symmetry spherical micelle packings. Specifically, exceptionally well-ordered and somewhat unusual C14 Laves phases form at high surfactant hydrations, in addition to C15 Laves, HCP, and BCC sphere packings. These phase behaviors stem from the specific surfactant conformations that arise from maximization of counterion-headgroup solvation while minimizing water-hydrophobic contact upon hydration, which influence the degree of counterion-headgroup electrostatic correlation and thus the supramolecular packing of the surfactants into LLCs. In the limit of high hydrations in these ternary surfactant/oil/


https://dx.doi.org/10.1021/acs.langmuir.9b03408
Langmuir 2020, 36, 2307−2321

water structured microemulsions, complex spherical micelle phases appear as a consequence of a drive to minimize local, molecular-level variations in surfactant headgroup-counterion solvation while maximizing global electrostatic cohesion across the supramolecular assembly. These findings suggest that the gemini dicarboxylate scaffold is robust platform that enables the formation of a wide variety of both polycontinuous network and structured droplet microemulsions, which may find future applications in the development of nanoporous molecular separations membranes and in therapeutic delivery and food science.

## ■ ASSOCIATED CONTENT

### Supporting Information

The Supporting Information is available free of charge at https://pubs.acs.org/doi/10.1021/acs.langmuir.9b03408.

SAXS data for **TMA-76** at $w_0$ = 2, **TMA-74_40** at $w_0$ = 28, **TMA-73_10** at $w_0$ = 30, **TMA-75_40** at $w_0$ = 12, network width plot, and electron density reconstruction method description and input file (PDF)

## ■ AUTHOR INFORMATION


### Corresponding Author

**Mahesh K. Mahanthappa** − *Department of Chemistry and Department of Chemical Engineering & Materials Science, University of Minnesota, Minneapolis, Minnesota 55455, United States;* orcid.org/0000-0002-9871-804X; Phone: +1 (608) 625-4599; Email: maheshkm@umn.edu

### Authors

**Carlos M. Baez-Cotto** − *Department of Chemistry, University of Minnesota, Minneapolis, Minnesota 55455, United States;* orcid.org/0000-0002-8785-7554

**Grayson L. Jackson** − *Department of Chemistry, University of Wisconsin, Madison, Wisconsin 53706, United States;* orcid.org/0000-0003-0663-3274

Complete contact information is available at: https://pubs.acs.org/10.1021/acs.langmuir.9b03408


### Notes

The authors declare no competing financial interest.

## ■ ACKNOWLEDGMENTS

We gratefully acknowledge financial support from National Science Foundation grant NSF-1608115 and NSF-1807330. Synchrotron SAXS analyses were conducted at Sector 12 of the Advanced Photon Source at Argonne National Laboratory, which is supported through the U.S. DOE Contract DE-AC02-06CH11357. Research results reported in this publication was supported by the Office of the Director, National Institutes of Health of the National Institutes of Health under Award Number S10OD011952. The content is solely the responsibility of the authors and does not necessarily represent the official views of the National Institutes of Health. We thank Ashish Jayaraman for insightful discussions.

## ■ REFERENCES


(1) Mezzenga, R.; Seddon, J. M.; Drummond, C. J.; Boyd, B. J.; Schröder-Turk, G. E.; Sagalowicz, L. Nature-Inspired Design and Application of Lipidic Lyotropic Liquid Crystals. *Adv. Mater.* **2019**, *31*, 1900818.

(2) Hyde, S. T. Chapter 16: Identification of Lyotropic Liquid Crystalline Mesophases. In *Handbook of Applied Surface and Colloid Chemistry*; Holmberg, K., Ed.; John Wiley & Sons, Ltd., New York, 2001; Vol. 2, p 299−332.

(3) Seddon, J. M. Structure of the Inverted Hexagonal ($H_{II}$) Phase, and Non-Lamellar Phase Transitions of Lipids. *Biochim. Biophys. Acta, Rev. Biomembr.* **1990**, *1031*, 1−69.

(4) Kato, T.; Mizoshita, N.; Kishimoto, K. Functional Liquid-Crystalline Assemblies: Self-Organized Soft Materials. *Angew. Chem., Int. Ed.* **2006**, *45*, 38−68.

(5) Fong, C.; Le, T.; Drummond, C. J. Lyotropic Liquid Crystal Engineering-Ordered Nanostructured Small Molecule Amphiphile Self-Assembly Materials by Design. *Chem. Soc. Rev.* **2012**, *41*, 1297−1322.

(6) Israelachvili, J. N. *Intermolecular and Surface Forces*, 3rd ed.; Academic Press: Burlington, MA, 2011; p 674.

(7) Mezzenga, R. Physics of Self-Assembly of Lyotropic Liquid Crystals. In *Self-Assembled Supramolecular Architectures: Lyotropic Liquid Crystals*; Garti, N., Somasundaran, P., Mezzenga, R., Eds.; John Wiley & Sons, Inc., Hoboken, NJ, 2012; p 1−20.

(8) Gin, D. L.; Bara, J. E.; Noble, R. D.; Elliott, B. J. Polymerized Lyotropic Liquid Crystal Assemblies for Membrane Applications. *Macromol. Rapid Commun.* **2008**, *29*, 367−389.

(9) Gin, D. L.; Pecinovsky, C. S.; Bara, J. E.; Kerr, R. L. Functional Lyotropic Liquid Crystal Materials. *Struct. Bonding (Berlin)* **2008**, *128*, 181−222.

(10) Pindzola, B. A.; Jin, J.; Gin, D. L. Cross-Linked Normal Hexagonal and Bicontinuous Cubic Assemblies Via Polymerizable Gemini Amphiphiles. *J. Am. Chem. Soc.* **2003**, *125*, 2940−2949.

(11) Hatakeyama, E. S.; Wiesenauer, B. R.; Gabriel, C. J.; Noble, R. D.; Gin, D. L. Nanoporous, Bicontinuous Cubic Lyotropic Liquid Crystal Networks Via Polymerizable Gemini Ammonium Surfactants. *Chem. Mater.* **2010**, *22*, 4525−4527.

(12) Huo, Q.; Margolese, D. I.; Stucky, G. D. Surfactant Control of Phases in the Synthesis of Mesoporous Silica-Based Materials. *Chem. Mater.* **1996**, *8*, 1147−1160.

(13) Han, Y.; Zhang, D. L.; Chng, L. L.; Sun, J. L.; Zhao, L.; Zou, X. D.; Ying, J. Y. A Tri-Continuous Mesoporous Material with a Silica Pore Wall Following a Hexagonal Minimal Surface. *Nat. Chem.* **2009**, *1*, 123−127.

(14) Han, L.; Che, S. Anionic Surfactant Templated Mesoporous Silicas (AMSS). *Chem. Soc. Rev.* **2013**, *42*, 3740−3752.

(15) Wan, Y.; Zhao, D. On the Controllable Soft-Templating Approach to Mesoporous Silicates. *Chem. Rev.* **2007**, *107*, 2821−2860.

(16) Caffrey, M.; Cherezov, V. Crystallizing Membrane Proteins Using Lipidic Mesophases. *Nat. Protoc.* **2009**, *4*, 706.

(17) Rummel, G.; Hardmeyer, A.; Widmer, C.; Chiu, M. L.; Nollert, P.; Locher, K. P.; Pedruzzi, I.; Landau, E. M.; Rosenbusch, J. P. Lipidic Cubic Phases: New Matrixes for the Three-Dimensional Crystallization of Membrane Proteins. *J. Struct. Biol.* **1998**, *121*, 82−91.

(18) Cherezov, V. Lipidic Cubic Phase Technologies for Membrane Protein Structural Studies. *Curr. Opin. Struct. Biol.* **2011**, *21*, 559−566.

(19) Leal, C.; Bouxsein, N. F.; Ewert, K. K.; Safinya, C. R. Highly Efficient Gene Silencing Activity of siRNA Embedded in a Nanostructured Gyroid Cubic Lipid Matrix. *J. Am. Chem. Soc.* **2010**, *132*, 16841−16847.

(20) Negrini, R.; Mezzenga, R. *p*H-Responsive Lyotropic Liquid Crystals for Controlled Drug Delivery. *Langmuir* **2011**, *27*, 5296−5303.

(21) Bouxsein, N. F.; McAllister, C. S.; Ewert, K. K.; Samuel, C. E.; Safinya, C. R. Structure and Gene Silencing Activities of Monovalent and Pentavalent Cationic Lipid Vectors Complexed with siRNA. *Biochemistry* **2007**, *46*, 4785−4792.

(22) Schröder-Turk, G. E.; de Campo, L.; Evans, M. E.; Saba, M.; Kapfer, S. C.; Varslot, T.; Grosse-Brauckmann, K.; Ramsden, S.; Hyde, S. T. Polycontinuous Geometries for Inverse Lipid Phases with

More Than Two Aqueous Network Domains. *Faraday Discuss.* **2013**, *161*, 215−247.
(23) Andersson, S.; Hyde, S. T.; Larsson, K.; Lidin, S. Minimal Surfaces and Structures: From Inorganic and Metal Crystals to Cell Membranes and Biopolymers. *Chem. Rev.* **1988**, *88*, 221−242.
(24) Wohlgemuth, M.; Yufa, N.; Hoffman, J.; Thomas, E. L. Triply Periodic Bicontinuous Cubic Microdomain Morphologies by Symmetries. *Macromolecules* **2001**, *34*, 6083−6089.
(25) Matsen, M. W.; Bates, F. S. Origins of Complex Self-Assembly in Block Copolymers. *Macromolecules* **1996**, *29*, 7641−7644.
(26) van 't Hag, L.; Gras, S. L.; Conn, C. E.; Drummond, C. J. Lyotropic Liquid Crystal Engineering Moving Beyond Binary Compositional Space - Ordered Nanostructured Amphiphile Self-Assembly Materials by Design. *Chem. Soc. Rev.* **2017**, *46*, 2705−2731.
(27) Phan, S.; Fong, W. K.; Kirby, N.; Hanley, T.; Boyd, B. J. Evaluating the Link between Self-Assembled Mesophase Structure and Drug Release. *Int. J. Pharm.* **2011**, *421*, 176−182.
(28) Sagalowicz, L.; Guillot, S.; Acquistapace, S.; Schmitt, B.; Maurer, M.; Yaghmur, A.; Campo, L. d.; Rouvet, M.; Leser, M.; Glatter, O. Oil-Loaded Monolinolein-Based Particles with Confined Inverse Discontinuous Cubic Structure *(Fd3m)*. *Langmuir* **2013**, *29*, 8222−8232.
(29) Wibroe, P. P.; Azmi, I. D. M.; Nilsson, C.; Yaghmur, A.; Moghimi, S. M. Citrem Modulates Internal Nanostructure of Glyceryl Monooleate Dispersions and Bypasses Complement Activation: Towards Development of Safe Tunable Intravenous Lipid Nanocarriers. *Nanomedicine* **2015**, *11*, 1909−1914.
(30) Salim, M.; Iskandar, W. F. N. W.; Patrick, M.; Zahid, N. I.; Hashim, R. Swelling of Bicontinuous Cubic Phases in Guerbet Glycolipid: Effects of Additives. *Langmuir* **2016**, *32*, 5552−5561.
(31) Guillot, S.; Moitzi, C.; Salentinig, S.; Sagalowicz, L.; Leser, M. E.; Glatter, O. Direct and Indirect Thermal Transitions from Hexosomes to Emulsified Micro-Emulsions in Oil-Loaded Monoglyceride-Based Particles. *Colloids Surf., A* **2006**, *291*, 78−84.
(32) Pouzot, M.; Mezzenga, R.; Leser, M.; Sagalowicz, L.; Guillot, S.; Glatter, O. Structural and Rheological Investigation of *Fd3m* Inverse Micellar Cubic Phases. *Langmuir* **2007**, *23*, 9618−9628.
(33) Guillot, S.; Salentinig, S.; Chemelli, A.; Sagalowicz, L.; Leser, M. E.; Glatter, O. Influence of the Stabilizer Concentration on the Internal Liquid Crystalline Order and the Size of Oil-Loaded Monolinolein-Based Dispersions. *Langmuir* **2010**, *26*, 6222−6229.
(34) Yaghmur, A.; Campo, L. d.; Sagalowicz, L.; Leser, M. E.; Glatter, O. Emulsified Microemulsions and Oil-Containing Liquid Crystalline Phases. *Langmuir* **2005**, *21*, 569−577.
(35) Yaghmur, A.; Campo, L. d.; Salentinig, S.; Sagalowicz, L.; Leser, M. E.; Glatter, O. Oil-Loaded Monolinolein-Based Particles with Confined Inverse Discontinuous Cubic Structure (*Fd3m*). *Langmuir* **2006**, *22*, 517−521.
(36) Vacklin, H. P.; Khoo, B. J.; Madan, K. H.; Seddon, J. M.; Templer, R. H. The Bending Elasticity of 1-Monoolein Upon Relief of Packing Stress. *Langmuir* **2000**, *16*, 4741−4748.
(37) Amar-Yuli, I.; Garti, N. Transitions Induced by Solubilized Fat into Reverse Hexagonal Mesophases. *Colloids Surf., B* **2005**, *43*, 72−82.
(38) Nazaruk, E.; Bilewicz, R.; Lindblom, G.; Lindholm-Sethson, B. Cubic Phases in Biosensing Systems. *Anal. Bioanal. Chem.* **2008**, *391*, 1569−1578.
(39) Vallooran, J. J.; Handschin, S.; Pillai, S. M.; Vetter, B. N.; Rusch, S.; Beck, H.-P.; Mezzenga, R. Lipidic Cubic Phases as a Versatile Platform for the Rapid Detection of Biomarkers, Viruses, Bacteria, and Parasites. *Adv. Funct. Mater.* **2016**, *26*, 181−190.
(40) Landau, E. M.; Rosenbusch, J. P. Lipidic Cubic Phases: A Novel Concept for the Crystallization of Membrane Proteins. *Proc. Natl. Acad. Sci. U. S. A.* **1996**, *93*, 14532−14535.
(41) Caffrey, M. On the Mechanism of Membrane Protein Crystallization in Lipidic Mesophases. *Cryst. Growth Des.* **2008**, *8*, 4244−4254.
(42) Kobilka, B. The Structural Basis of G-Protein-Coupled Receptor Signaling (Nobel Lecture). *Angew. Chem., Int. Ed.* **2013**, *52*, 6380−6388.
(43) Zabara, A.; Mezzenga, R. Controlling Molecular Transport and Sustained Drug Release in Lipid-Based Liquid Crystalline Mesophases. *J. Controlled Release* **2014**, *188*, 31−43.
(44) Drummond, C. J.; Fong, C. Surfactant Self-Assembly Objects as Novel Drug Delivery Vehicles. *Curr. Opin. Colloid Interface Sci.* **1999**, *4*, 449−456.
(45) Barriga, H. M. G.; Tyler, A. I. I.; McCarthy, N. L. C.; Parsons, E. S.; Ces, O.; Law, R. V.; Seddon, J. M.; Brooks, N. J. Temperature and Pressure Tuneable Swollen Bicontinuous Cubic Phases Approaching Nature's Length Scales. *Soft Matter* **2015**, *11*, 600−607.
(46) Kim, H.; Song, Z.; Leal, C. Super-Swelled Lyotropic Single Crystals. *Proc. Natl. Acad. Sci. U. S. A.* **2017**, *114*, 10834−10839.
(47) Leung, S. S. W.; Leal, C. The Stabilization of Primitive Bicontinuous Cubic Phases with Tunable Swelling over a Wide Composition Range. *Soft Matter* **2019**, *15*, 1269−1277.
(48) Israelachvili, J. N.; Mitchell, D. J.; Ninham, B. W. Theory of Self-Assembly of Hydrocarbon Amphiphiles into Micelles and Bilayers. *J. Chem. Soc., Faraday Trans. 2* **1976**, *72*, 1525−1568.
(49) Shearman, G. C.; Ces, O.; Templer, R. H.; Seddon, J. M. Inverse Lyotropic Phases of Lipids and Membrane Curvature. *J. Phys.: Condens. Matter* **2006**, *18*, S1105−S1124.
(50) Pindzola, B. A.; Hoag, B. P.; Gin, D. L. Polymerization of a Phosphonium Diene Amphiphile in the Regular Hexagonal Phase with Retention of Mesostructure. *J. Am. Chem. Soc.* **2001**, *123*, 4617−4618.
(51) Pindzola, B. A.; Jin, J.; Gin, D. L. Cross-Linked Normal Hexagonal and Bicontinuous Cubic Assemblies Via Polymerizable Gemini Amphiphiles. *J. Am. Chem. Soc.* **2003**, *125*, 2940−2949.
(52) Gin, D. L.; Noble, R. D. Designing the Next Generation of Chemical Separation Membranes. *Science* **2011**, *332*, 674−676.
(53) In, M.; Zana, R. Phase Behavior of Gemini Surfactants. *J. Dispersion Sci. Technol.* **2007**, *28*, 143−154.
(54) Sorenson, G. P.; Coppage, K. L.; Mahanthappa, M. K. Unusually Stable Aqueous Lyotropic Gyroid Phases from Gemini Dicarboxylate Surfactants. *J. Am. Chem. Soc.* **2011**, *133*, 14928−14931.
(55) Perroni, D. V.; Baez-Cotto, C. M.; Sorenson, G. P.; Mahanthappa, M. K. Linker Length-Dependent Control of Gemini Surfactant Aqueous Lyotropic Gyroid Phase Stability. *J. Phys. Chem. Lett.* **2015**, *6*, 993−998.
(56) Sorenson, G. P.; Schmitt, A. K.; Mahanthappa, M. K. Discovery of a Tetracontinuous, Aqueous Lyotropic Network Phase with Unusual 3D-Hexagonal Symmetry. *Soft Matter* **2014**, *10*, 8229−8235.
(57) Kunieda, H.; Masuda, N.; Tsubone, K. Comparison between Phase Behavior of Anionic Dimeric (Gemini-Type) and Monomeric Surfactants in Water and Water-Oil. *Langmuir* **2000**, *16*, 6438−6444.
(58) Jennings, J.; Green, B.; Mann, T. J.; Guymon, C. A.; Mahanthappa, M. K. Nanoporous Polymer Networks Templated by Gemini Surfactant Lyotropic Liquid Crystals. *Chem. Mater.* **2018**, *30*, 185−196.
(59) Porcar, L.; Hamilton, W. A.; Butler, P. D.; Warr, G. G. Scaling of Structural and Rheological Response of L3 Sponge Phases in the "Sweetened" Cetylpyridinium/Hexanol/Dextrose/Brine System. *Langmuir* **2003**, *19*, 10779−10794.
(60) Baez-Cotto, C. M.; Mahanthappa, M. K. Micellar Mimicry of Intermetallic C14 and C15 Laves Phases by Aqueous Lyotropic Selfassembly. *ACS Nano* **2018**, *12*, 3226−3234.
(61) Yaghmur, A.; Rappolt, M. Chapter Five: The Micellar Cubic *Fd3m* Phase: Recent Advances in the Structural Characterization and Potential Applications. In *Advances in Planar Lipid Bilayers and Liposomes*; Iglic, A., Kulkarni, C., Eds.; Academic Press, Inc., Waltham, MA, 2013; Vol. *18*, p 111−146.
(62) de Geyer, A.; Guillermo, A.; Rodriguez, V.; Molle, B. Evidence for Spontaneous Formation of Three-Dimensionally Periodic Cellular Structures in a Water/Oil/Surfactant/Alcohol System. *J. Phys. Chem. B* **2000**, *104*, 6610−6617.


https://dx.doi.org/10.1021/acs.langmuir.9b03408
*Langmuir* 2020, 36, 2307−2321

(63) Kim, K.; Schulze, M. W.; Arora, A.; Lewis, R. M.; Hillmyer, M. A.; Dorfman, K. D.; Bates, F. S. Thermal Processing of Diblock Copolymer Melts Mimics Metallurgy. *Science* **2017**, *356*, 520−523.
(64) Jayaraman, A.; Mahanthappa, M. K. Counterion-Dependent Access to Low-Symmetry Lyotropic Sphere Packings of Ionic Surfactant Micelles. *Langmuir* **2018**, *34*, 2290−2301.
(65) Zhang, J.; Sides, S.; Bates, F. S. Ordering of Sphere Forming SISO Tetrablock Terpolymers on a Simple Hexagonal Lattice. *Macromolecules* **2012**, *45*, 256−265.
(66) Hyde, S. T.; Fogden, A. Hexagonal Mesophases. Honeycomb, Froth, Mesh, or Sponge? *Prog. Colloid Polym. Sci.* **1998**, *108*, 139−152.
(67) Mondal, J.; Mahanthappa, M.; Yethiraj, A. Self-Assembly of Gemini Surfactants: A Computer Simulation Study. *J. Phys. Chem. B* **2013**, *117*, 4254−4262.
(68) Mantha, S.; McDaniel, J. G.; Perroni, D. V.; Mahanthappa, M. K.; Yethiraj, A. Electrostatic Interactions Govern "Odd/Even" Effects in Water-Induced Gemini Surfactant Self-Assembly. *J. Phys. Chem. B* **2017**, *121*, 565−576.
(69) Kunieda, H.; Ozawa, K.; Huang, K.-L. Effect of Oil on the Surfactant Molecular Curvatures in Liquid Crystals. *J. Phys. Chem. B* **1998**, *102*, 831−838.
(70) Chen, H.; Jin, C. Competition Brings out the Best: Modelling the Frustration between Curvature Energy and Chain Stretching Energy of Lyotropic Liquid Crystals in Bicontinuous Cubic Phases. *Interface Focus* **2017**, *7*, 20160114.
(71) Rappolt, M.; Cacho-Nerin, F.; Morello, C.; Yaghmur, A. How the Chain Configuration Governs the Packing of Inverted Micelles in the Cubic Fd3m-Phase. *Soft Matter* **2013**, *9*, 6291−6300.
(72) Lee, S.; Leighton, C.; Bates, F. S. Sphericity and Symmetry Breaking in the Formation of Frank-Kasper Phases from One Component Materials. *Proc. Natl. Acad. Sci. U. S. A.* **2014**, *111*, 17723−17731.
(73) Kim, S. A.; Jeong, K.-J.; Yethiraj, A.; Mahanthappa, M. K. Low-Symmetry Sphere Packings of Simple Surfactant Micelles Induced by Ionic Sphericity. *Proc. Natl. Acad. Sci. U. S. A.* **2017**, *114*, 4072−4077.
(74) Alexander, S.; McTague, J. Should All Crystals Be BCC? Landau Theory of Solidification and Crystal Nucleation. *Phys. Rev. Lett.* **1978**, *41*, 702−705.
(75) Grason, G. M. The Packing of Soft Materials: Molecular Asymmetry, Geometric Frustration and Optimal Lattices in Block Copolymer Melts. *Phys. Rep.* **2006**, *433*, 1−64.
(76) Reddy, A.; Buckley, M. B.; Arora, A.; Bates, F. S.; Dorfman, K. D.; Grason, G. M. Stable Frank-Kasper Phases of Self-Assembled, Soft Matter Spheres. *Proc. Natl. Acad. Sci. U. S. A.* **2018**, *115*, 10233−10238.
(77) Ungar, G.; Liu, Y.; Zeng, X.; Percec, V.; Cho, W.-D. Giant Supramolecular Liquid Crystal Lattice. *Science* **2003**, *299*, 1208−1211.
(78) Balagurusamy, V. S. K.; Ungar, G.; Percec, V.; Johansson, G. Rational Design of the First Spherical Supramolecular Dendrimers Self-Organized in a Novel Thermotropic Cubic Liquid-Crystalline Phase and the Determination of Their Shape by X-Ray Analysis. *J. Am. Chem. Soc.* **1997**, *119*, 1539−1555.
(79) Jayaraman, A.; Zhang, D. Y.; Dewing, B. L.; Mahanthappa, M. K. Path-Dependent Preparation of Complex Micelle Packings of a Hydrated Diblock Oligomer. *ACS Cent. Sci.* **2019**, *5*, 619−628.
(80) Hynninen, A.-P.; Thijssen, J. H. J.; Vermolen, E. C. M.; Dijkstra, M.; van Blaaderen, A. Self-Assembly Route for Photonic Crystals with a Bandgap in the Visible Region. *Nat. Mater.* **2007**, *6*, 202−205.
(81) Petříček, V.; Dušek, M.; Palatinus, L. Crystallographic Computing System *JANA2006*: General Features. *Z. Kristallogr. - Cryst. Mater.* **2014**, *229*, 345−352.
(82) Palatinus, L.; Chapuis, G. *SUPERFLIP*-A Computer Program for the Solution of Crystal Structures by Charge Flipping in Arbitrary Dimensions. *J. Appl. Crystallogr.* **2007**, *40*, 786−790.


https://dx.doi.org/10.1021/acs.langmuir.9b03408
*Langmuir* 2020, 36, 2307−2321